USGS
science for a changing world

Prepared in cooperation with Northern Arizona University

Channel Mapping River Miles 29–62 of the Colorado River in Grand Canyon National Park, Arizona, May 2009

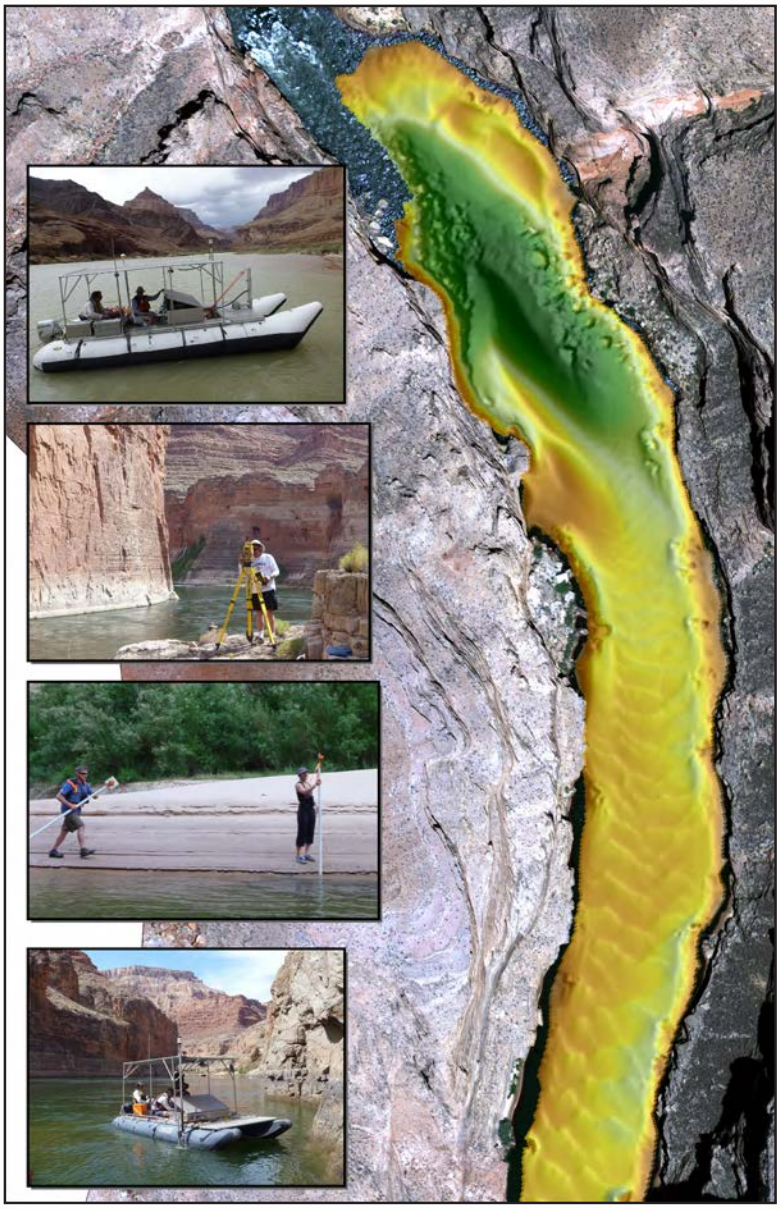

Open-File Report 2017–1030

U.S. Department of the Interior
U.S. Geological Survey

Cover: One-meter digital elevation model in study area at River Mile 36.4, Colorado River, Grand Canyon National Park, Arizona, overlain on orthophotograph, May 2009.

Insets: Total station surveying and sonar survey vessels in study area. Photographs by Joseph E. Hazel, Jr., U.S. Geological Survey, 2009.

Channel Mapping River Miles 29–62 of the Colorado River in Grand Canyon National Park, Arizona, May 2009

By Matt Kaplinski, Joseph E. Hazel, Jr., Paul E. Grams, Keith Kohl, Daniel D. Buscombe, and Robert B. Tusso

Prepared in cooperation with Northern Arizona University

Open-File Report 2017–1030

U.S. Department of the Interior
U.S. Geological Survey

U.S. Department of the Interior
RYAN K. ZINKE, Secretary

U.S. Geological Survey
William H. Werkheiser, Acting Director

U.S. Geological Survey, Reston, Virginia: 2017

Suggested citation:
Kaplinski, M., Hazel, J.E., Jr., Grams, P.E., Kohl, Keith, Buscombe, D.D., and Tusso, R.B., 2017, Channel mapping river miles 29–62 of the Colorado River in Grand Canyon National Park, Arizona, May 2009: U.S. Geological: Survey Open-File Report 2017–1030, 35 p., https://doi.org/10.3133/ofr20171030.

ISSN 2331-1258 (online)

Contents

Abstract 1
Introduction 1
  Study Area, Place Names, and Units 3
  Study Reach 3
Data Collection and Processing 3
  Geodetic Control Network 4
  Conventional Total Station Surveys 4
  Bathymetric Surveys 6
  Grain-Size Surveys 7
  Bed-Sediment Classification 9
Digital Elevation Models 9
Digital Elevation Model Uncertainty 11
  Measurement Uncertainty 11
  Fuzzy Inference System Elevation Uncertainty Model 14
    Fuzzy Inference System Input 17
      Slope 19
      Roughness 19
      Interpolation Uncertainty 21
      Point Density 23
    Fuzzy Inference System Output 25
Results 32
Summary 32
Acknowledgments 33
References Cited 33

Figures

Figure 1. Map showing location of study reach and sediment and U.S. Geological Survey streamgages, Colorado River, Grand Canyon National Park, Arizona 2
Figure 2. Photographs of total station surveying in study area, Colorado River, Grand Canyon National Park, Arizona 5
Figure 3. Photographs of sonar survey vessels in study area, Grand Canyon National Park, Arizona 6
Figure 4. Photographs of underwater microscope system deployment in study area, Colorado River, Grand Canyon National Park, Arizona 8
Figure 5. Orthoimages showing steps in digital terrain model construction for study area, Colorado River, Grand Canyon National Park, Arizona 10
Figure 6. Results of multibeam survey performance test comparing the vertical difference between a check line with a reference surface at river mile 36.4, Colorado River, Grand Canyon National Park, Arizona 12
Figure 7. Singlebeam survey cross-line checks at river mile 42.5, Colorado River, Grand Canyon National Park, Arizona 13
Figure 8. Diagram of fuzzy inference system model for multibeam sonar survey areas showing input and output membership functions 15
Figure 9. Diagram of fuzzy inference system model for singlebeam sonar survey areas showing input and output membership functions 16

Figure 10. Diagram of fuzzy inference system for total station survey areas showing input and output membership functions. Inputs are slope, interpolation error, and point density 17
Figure 11. Images showing digital elevation model (DEM), slope, point density, interpolation error, and roughness raster surfaces used to derive the fuzzy inference system input membership functions, for an approximately 0.5-kilometer section of study reach located at river mile 34.9, Colorado River, Grand Canyon National Park, Arizona 18
Figure 12. Image showing 1-meter slope raster for an approximately 0.5-kilometer section of study reach and plots for each data-collection area with histograms of distribution of cell values and the input membership function used in the fuzzy inference system model, on the Colorado River, Grand Canyon National Park, Arizona 20
Figure 13. Image showing 1-meter roughness raster for an approximately 0.5-kilometer section of the study reach and plots for each data-collection area with histogram of distribution of cell values and the input membership function used in fuzzy inference system model, on the Colorado River, Grand Canyon National Park, Arizona 21
Figure 14. Image showing 1-meter interpolation uncertainty raster for an approximately 0.5-kilometer section of study reach and plots for each data-collection area with histograms of distribution of cell values and the input membership function used in fuzzy inference system model, on the Colorado River, Grand Canyon National Park, Arizona 22
Figure 15. Image showing 1-meter point density raster for an approximately 0.5-kilometer section of study reach and plots for each data-collection area with histograms of distribution of cell values and the input membership function used in the fuzzy inference system model, on the Colorado River, Grand Canyon National Park, Arizona 24
Figure 16. Image showing standard deviation of soundings within each 1-meter cell and graph showing distribution, and summary statistics of dataset from multibeam survey collected at river mile 34.9, Colorado River, Grand Canyon National Park, Arizona 26
Figure 17. Image of fuzzy inference system (FIS) elevation uncertainty output, and graphs showing distributions and summary statistics of dataset segregated by survey type, for the study reach on the Colorado River, Grand Canyon National Park, Arizona 27

Tables

Table 1. Three-input fuzzy inference system ruleset for total station surveys 28
Table 2. Three-input fuzzy inference system ruleset for singlebeam sonar surveys 29
Table 3. Four-input fuzzy inference system ruleset for multibeam sonar surveys 30

Conversion Factors

U.S. customary units to International System of Units

Multiply	By	To obtain
	Length	
foot (ft)	0.3048	meter (m)
mile (mi)	1.609	kilometer (km)
	Flow rate	
cubic foot per second (ft^3/s)	0.02832	cubic meter per second (m^3/s)

International System of Units to U.S. customary units

Multiply	By	To obtain
	Length	
millimeter (mm)	0.03937	inch (in.)
centimeter (cm)	0.3937	inch (in.)
meter (m)	3.281	foot (ft)
kilometer (km)	0.6214	mile (mi)
	Area	
square meter (m^2)	10.76	square foot (ft^2)
	Sound velocity	
meter per second (m/s)	3.281	foot per second (ft/s)
	Mass	
kilogram (kg)	2.205	pound avoirdupois (lb)

Datums

Vertical coordinate information is referenced to the Geodetic Reference System 1980 (GRS 80) ellipse defined by the North American Datum of 1983 (NAD 83 (2011).

Horizontal coordinate information is referenced to NAD 83 (2011) and projected to State Plane Coordinate System, Arizona Central Zone, in meters.

Elevation, as used in this report, refers to distance above the Geodetic Reference System 1980 (GRS 80) ellipse defined by the North American Datum of 1983 (NAD 83) (2011).

Abbreviations

DEM	digital elevation model
GCD	Glen Canyon Dam
FIS	fuzzy inference system
GNSS	Global Navigation Satellite System
GRCA	Grand Canyon National Park
Hz	hertz
kHz	kilohertz
MB	multibeam (sonar)
MAE	mean absolute elevation difference
MAX	maximum value of population
MBES	multibeam echo sounder
ME	mean elevation difference
MIN	Maximum value of population
MF	fuzzy inference system membership function
N	number of observations
NAD 83	North American Datum of 1983
RM	river mile
RMSE	root mean square error
SB	singlebeam (sonar)
SD	standard deviation
TIN	triangular irregular network
TS	total-station
USGS	U.S. Geological Survey

Channel Mapping River Miles 29–62 of the Colorado River in Grand Canyon National Park, Arizona, May 2009

By Matt Kaplinski[1], Joseph E. Hazel[1], Paul E. Grams[2], Keith Kohl[2], Daniel D. Buscombe[1], and Robert B. Tusso[2]

Abstract

Bathymetric, topographic, and grain-size data were collected in May 2009 along a 33-mi reach of the Colorado River in Grand Canyon National Park, Arizona. The study reach is located from river miles 29 to 62 at the confluence of the Colorado and Little Colorado Rivers. Channel bathymetry was mapped using multibeam and singlebeam echosounders, subaerial topography was mapped using ground-based total-stations, and bed-sediment grain-size data were collected using an underwater digital microscope system. These data were combined to produce digital elevation models, spatially variable estimates of digital elevation model uncertainty, georeferenced grain-size data, and bed-sediment distribution maps. This project is a component of a larger effort to monitor the status and trends of sand storage along the Colorado River in Grand Canyon National Park. This report documents the survey methods and post-processing procedures, digital elevation model production and uncertainty assessment, and procedures for bed-sediment classification, and presents the datasets resulting from this study.

Introduction

Sandbars and other sandy deposits in and along the Colorado River in Grand Canyon National Park (GRCA), Arizona, are an integral part of the natural riverscape, and are important for riparian habitat, native fish habitat, protection of archeological sites, and recreation (Rubin and others, 2002; Wright and others, 2005). Following closure of Glen Canyon Dam (GCD) in 1963, the supply of sand at the upstream boundary of GRCA, located at Lees Ferry (fig. 1), was reduced by about 94 percent (Topping and others, 2000). In response to this reduction in sand supply and the alteration of the natural hydrograph by dam operations (Topping and others, 2003), the number and size of sandbars in Marble Canyon and the upstream part of the Grand Canyon have substantially decreased in the post-dam era (Schmidt and Graf, 1990; Schmidt and others, 2004). The current strategy to restore and maintain eroded sandbars is to release artificial, controlled floods (hereinafter referred to as “high flows”) from GCD, timed and triggered by tributary sediment inputs (Wright and others, 2008; Mueller and others, 2014:, Grams and others, 2015). High flows have been released in 1996, 2004, 2008, 2012, 2013, and 2014.

[1]Northern Arizona University.
[2]U.S. Geological Survey.

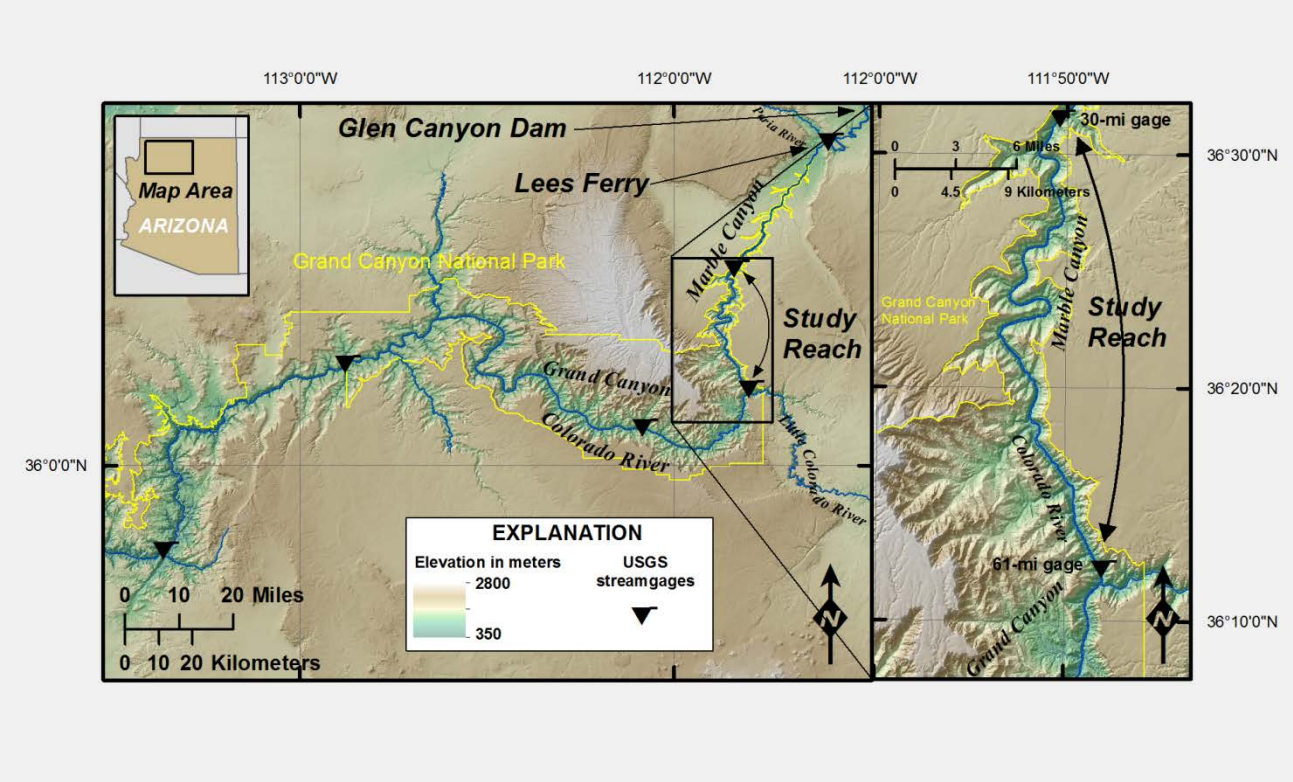

Figure 1. Map showing location of study reach and sediment and U.S. Geological Survey streamgages, Colorado River, Grand Canyon National Park, Arizona.

A major outstanding question is whether repeated high flows conducted under sediment-enriched conditions can result in the rebuilding and maintenance of sandbars over annual to decadal time scales. Recent work has shown that most of the sand is stored in the low-elevation (here, taken to be less than the stage elevation associated with a discharge of 8,000 ft^3/s) parts of these sandbars deposited in lateral flow recirculation eddies and in the main channel adjacent to eddies (Hazel and others, 2008; Grams and others, 2013). Determining whether sand storage in the Colorado River in the Grand Canyon is increasing, decreasing, or stable requires repeat measurements of sand storage. For these reasons, fine sediment monitoring consists of measurements of channel and eddy sand storage in reaches between the U.S. Geological Survey (USGS) streamgages (fig. 1).

This report describes topographic, bathymetric, and grain-size surveys conducted in May 2009 in a 33-mi (53-km) study reach (fig. 1), the production of digital elevation models (DEMs) of the study reach, the procedures used to estimate the uncertainty associated with the DEMs, and the production of bed-sediment distribution maps (fig. 1). Mapping of the segment described in this report was repeated in 2012 and changes in fine sediment storage volume will be computed and analyzed for the detection of trends. This report is the first in a series of reports that will describe subsequent mapping efforts. The results obtained from the surveys also will be used to provide input to sediment transport modeling efforts and to provide insights into the geomorphic framework of the river corridor.

Study Area, Place Names, and Units

The study area is a segment of the Colorado River corridor in GCRA in northern Arizona (fig. 1). Locations discussed in this report are referenced by the USGS Grand Canyon Monitoring and Research Center river mile (RM) system, which is distance in miles along the channel centerline downstream of Lees Ferry, Arizona (U.S. Geological Survey, 2006). Distances are referenced in both miles and kilometers. Lees Ferry (RM 0) is located 15.5 mi (21.4 km) downstream of GCD (not shown in fig. 1), and 1 mi (1.6 km) upstream of the mouth of the Paria River and the northeastern boundary of GCRA (fig. 1). Units of streamflow are reported in cubic feet per second.

In order to integrate spatial datasets from different sources in a composite DEM, all topographic and bathymetric data were projected to the Arizona Central Zone of the State Plane Coordinate System of 1983, in meters (Stem, 1989) and constrained to the 2011 national adjustment of the North American Datum of 1983 (NAD 83). Elevations are referenced to distances above the NAD 83 ellipse. Elevations are not referenced to the North American Vertical Datum of 1988 (NAVD 88) because the national geoid model (currently GEOID12a) does not incorporate sufficient gravity measurements in the Grand Canyon region to account for the large variation in crustal mass along the river corridor (Saleh and others, 2003).

Study Reach

Topographic and bathymetric data were collected along an approximately 33-mi (53 km) study reach (fig. 1). The 270-mi river corridor in GRCA is subdivided into the Marble Canyon and the Grand Canyon, with the Marble Canyon extending from the mouth of the Paria River (RM 1) to the confluence with the Little Colorado River (RM 62). The study reach in this report is located entirely within Marble Canyon. This reach corresponds to the segment of channel that lies between USGS streamgages at RMs 30 (09402500) and 61 (09404200), which measure stage, streamflow, and suspended-sediment concentration at 15-minute intervals. Upon completion of a repeat survey for the study reach (completed in 2012 for this reach), all components of the sediment budget (for example, the sediment influx at the upstream streamgage, the sediment efflux at the downstream streamgage, and the change in storage between the streamgages) will have been measured directly. This reach also includes several existing bathymetric datasets (Wright and Kaplinski, 2011; Grams and others, 2013; and Kaplinski and others, 2014), and, thus, comparison between the 2009 presented here and these previous surveys will be possible.

Data Collection and Processing

The sections that follow describe the methods used to survey and process the data collected on a research river trip conducted from May 6 to May 19, 2009. Channel bathymetry was mapped by multibeam (MB) and singlebeam (SB) sonar, and subaerial topography was mapped by ground-based total-station (TS) surveys. The MB sonar dataset also contains georeferenced backscatter and auxiliary sonar information that was used to classify bed sediment in those areas mapped by MB sonar, at the same resolution as the bathymetry. Results from the surveys are integrated in a Geographic Information System to construct DEMs, uncertainty surfaces, and bed-sediment classification maps.

Geodetic Control Network

A network of geodetic control benchmarks was established along the canyon rim and the river corridor. Coordinates of benchmarks along the north and south rims were computed through multiple, independent static Global Navigation Satellite System (GNSS) observations using the procedures described by Zilkoski and others (1997) and published in the National Spatial Reference System using National Geodetic Survey protocols (Doyle, 1994). The control network for topographic and bathymetric mapping along the Colorado River corridor in the Grand Canyon includes both GNSS and TS measurements. Terrestrial, TS measurements to and from monuments along the river corridor have been constrained to the globally derived GNSS positions using a least squares adjustment. Network accuracy of the GNSS-derived benchmarks in relation to the NAD 83 ellipse was 0.004 m horizontal and 0.029 m vertical at 68-percent confidence, and 0.7 cm horizontal and 5.2 cm vertical at 95-percent confidence. Network accuracy of the TS-derived benchmarks was 1.5 cm horizontal and 2.7 cm vertical at 68-percent confidence, and 3.3 cm horizontal and 5.2 cm vertical at 95-percent confidence.

In the 33-mi study reach, there are 64 GNSS-derived and 119 TS-derived benchmarks that comprise the control network; 85 of these were occupied with total stations for this study. Additionally, the network includes May 2009 TS measurements to and from 42 temporary benchmark locations established and used for bathymetric mapping.

Conventional Total Station Surveys

TS surveys were used to:

- Measure distance between control network benchmarks (fig. 2);
- Position temporary benchmarks;
- Position sand camera photograph locations; and
- Survey the eddy, sandbar, and riverbank topography.

TS surveys use manually operated electronic total stations (for example, Topcon™ GTS-313, Topcon™ GPT-2003, Topcon™ GTS-233, or similar). An operator plumbs the instrument on a tripod over a control network monument and orients its direction by referencing a tripod and prism over a second known benchmark (for example, a backsight), typically at a distance of 600 m or less. Several survey crews (1 instrument operator and 1–3 rodmen) operate simultaneously by “leapfrogging” benchmark occupations in a downstream direction.

Figure 2. Photographs of total station surveying in study area, Colorado River, Grand Canyon National Park, Arizona. *A*, Total station established over geodetic control benchmark. *B*, Rodmen surveying edge of water using stadia rod and prism. Photographs by Joseph E. Hazel, Jr., U.S. Geological Survey, 2009.

Prior to all TS data collection, multiple sets of measurements are made from the instrument to a second network position (for example, a backsight necessary for a reference azimuth). Horizontal and zenith angles (1-arcsecond precision; 1/3,600 degree) and slope distances (1-mm precision) to the backsight are recorded in both forward and reverse faces of the instrument. Resulting coordinates are computed and field results are immediately compared to the geodetic network coordinates. This initial quality control:

- Ensures the instrument is able to repeatedly and precisely index a target,
- Validates proper collimation of the instrument and that the crosshairs are level and plumb,
- Records results of the instrument collimation, and
- Verifies that the instrument operator is referencing correct benchmark coordinates.

The local or relative accuracy of TS surveys is defined by the difference between GNSS and TS positions. Statistical analysis of these data shows that about 68 percent of the field measurements are within 0.011 m horizontal and 0.012 m vertical of GNSS results, and 95 percent of these measurements are within 0.031 m horizontal and 0.034 m vertical of GNSS results.

Topographic measurements are made by sighting to a reflecting prism target mounted on portable survey rods operated by one or more field assistants (rodmen). TS surveys capture sandbars, water-surface elevations, and shallow (for example , less than 1 m) offshore locations. Topographic breaklines are collected along continuous features such as dune crests, terraces, and water's edge; and these sharp breaks in topography and (or) linear features are linked during surveying to ensure proper terrain modelling.

Bathymetric Surveys

Bathymetric surveys were collected using both MB and SB sonar systems deployed on motorized rafts (fig. 3). The MB mapping system was mounted on the *R.V. Greg Sponenbergh*, a 7-m inflatable pontoon (snout) raft powered by a 50-horsepower 4-stroke outboard motor (fig. 3*A*). The SB mapping system was mounted on the *R.V. Frank Protiva*, a 5-m inflatable pontoon (mini-snout) raft, also powered by a 50-horsepower 4-stroke outboard motor (fig. 3*B*).

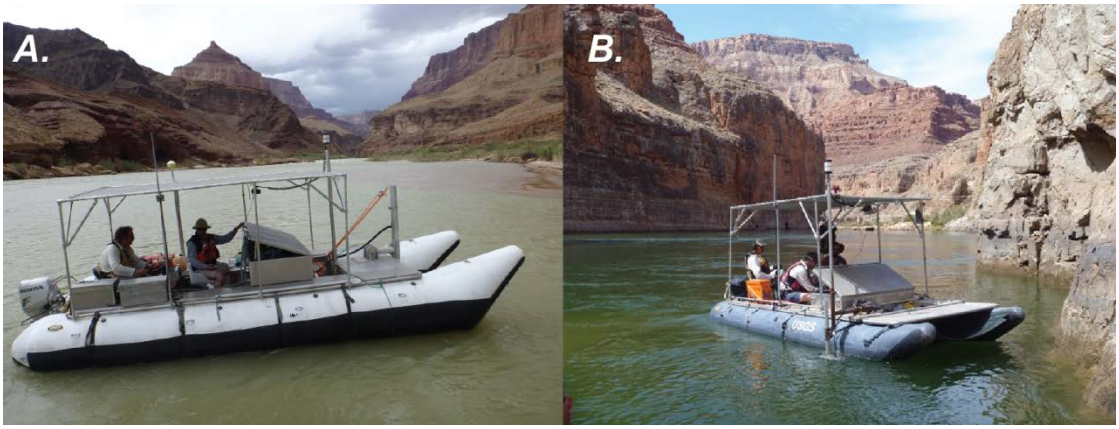

Figure 3. Photographs of sonar survey vessels in study area, Grand Canyon National Park, Arizona. *A*, multibeam survey vessel *R.V. Greg Sponenbergh*. *B*, Singlebeam survey vessel *R.V. Frank Protiva*. Photographs by Joseph E. Hazel, Jr., U.S. Geological Survey, 2009.

The MB system used a 455 kilohertz (kHz) RESON® Seabat™ 8125 multibeam echo sounder (MBES) mounted on the bow of the survey vessel frame to collect bed surface elevation and acoustic backscatter data. A sound velocity probe (RESON® SV-71) is attached to the MBES head to continuously measure the speed of sound near the sonar transmit and receive arrays. Periodic casts of a sound velocity probe show that the water column is very well mixed, varying only by about 0.2 m/s from the sound velocity measured at the surface (Buscombe and others, 2014a). A Teledyne TSS® motion heading and reference system was used to collect roll, pitch, and heading information. The SB system used an Odom® CV-100 singlebeam echo sounder with a 200-kHz transducer mounted off the starboard bow of the survey vessel. Both bathymetry systems used a line-of-sight, range-azimuth navigation system (Kaplinski and others, 2009). The range-azimuth system uses a robotic TS (Trimble® SPS930) located on a control network benchmark to track the position and elevation of the survey vessel at a maximum range from the instrument of about 500 m. The raw positioning information (slope distance, and horizontal and vertical angles) is referenced to the benchmark location and transmitted to the survey vessel by radio modem at a rate of 20 hertz (Hz). The measured depths are subtracted from the elevation of the transducer to derive bed elevations. This practice of surveying in elevation removes the uncertainty associated with heave and dynamic heave, whereas both depth and water surface elevation are recoverable from the data. The accuracy of the Trimble® SPS930 to a target 100 m from the instrument moving at 1 m/s is specified by the manufacturer as ±0.002 m for horizontal, vertical, and slope distance measurements. HYPACK®/HYSWEEP® software was used to collect and process survey data.

The general strategy for any survey was to survey most of the area with the MB system, then follow with the SB system (fig 3*A*). In order to minimize the risk of affecting the sonar transducer, we restricted the MB surveys to depths of about 2 m underneath the sonar head whenever possible. MB surveys were collected without planned line files, and most of the remaining area between the MB coverage and the shoreline was surveyed with the SB system, with particular emphasis on shallow sandy areas in lateral recirculation zones (for example , eddies). Upon completion of a MB survey, a preliminary map of the area was generated to define the channel topography and the extent of MB coverage. This preliminary map was transferred to the SB system operator to determine the extent of SB mapping necessary to ensure continuous coverage of the survey area. The SB system also was used to survey the entire channel in a few particularly shallow stretches (that is, less than about 2–3 m in depth) of the study reach. For these full-channel SB surveys, data were collected along planned lines with 15 m spacing in the cross-stream direction and about 15 m spacing in the stream-wise direction.

Upon completion of the surveys, the bathymetric data were processed and edited using the HYPACK®/HYSWEEP® software suite to correct any survey blunders (most commonly, incorrect coordinates of robotic TS positions) and to identify and remove erroneous soundings. Editing the bathymetric data, particularly the MB soundings, requires expert judgement, and was the most time-consuming aspect of data processing. Sonar data collected in the Colorado River are inherently "noisy" because of a combination of steep slopes, topographic complexity, side-lobe effects, multipath effects, water-column targets (air bubble, suspended particles, fish, etc.), and ambient high-frequency noise. Identification and removal of soundings that do not represent the channel bed require that all soundings are visually inspected and manually edited. We investigated various automatic filters and determined that no combination of filters properly identified all outliers; thus, visual inspection and removal of outliers produced the most accurate representation of channel bathymetry. In fact, most automated filtering algorithms increased processing time by misidentifying accurate soundings as outliers and subsequently removing those data; this was particularly common in rocky areas. Therefore, we preferred to manually inspect and edit data. Upon completion of editing, the MB soundings were decimated by calculating the median elevation of soundings within 0.25-m and 1.0-m square grid cells and were output as human-readable (ascii) format files. SB data were filtered to only include one median elevation per meter along each survey trackline and were output as ascii text files. The 1-m decimated datasets from both the MB and SB systems were used to construct the bathymetry portion of the DEMs.

Grain-Size Surveys

Bed-sediment imagery was collected to both directly measure grain size and to ground truth the automated remote classification of bed sediment using acoustic backscatter derived from multibeam sonar. Images were collected using an underwater digital microscope system developed by USGS (fig 4; Chezar and Rubin, 2004; Rubin and others, 2007). The system uses a digital plumbing inspection camera housed inside an aluminum cylinder with a glass window at one end. The camera is fixed at macro focus on the outer face of the window, and this unit is placed inside a 0.23-m-diameter, 45-kg steel split overhaul ball, with the window flush on the underside of the ball (fig. 4*B*). Upon contact with the bed, the window presses into the sand, and the operator collects a 720 × 480 pixel still image from the video feed using a Sony® GV-HD700E digital video deck. The camera and ball were lowered through the water column to the river bed using a USGS B-56 Sounding Reel mounted on the bow of a 11-m, four-pontoon motor raft, powered by a 30-horsepower outboard motor (fig. 4*A*).

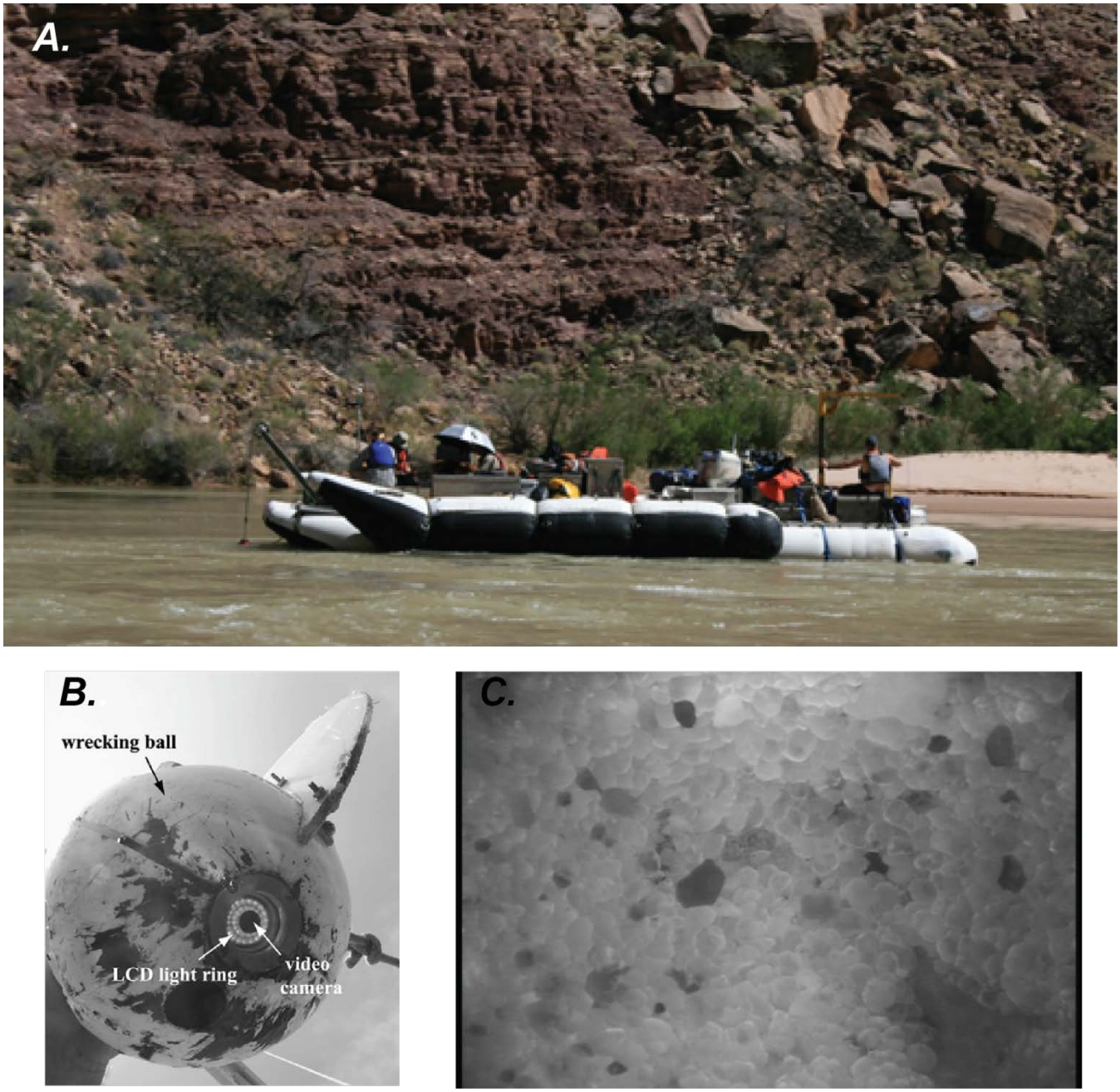

Figure 4. Photographs of underwater microscope system (Rubin and others, 2007) deployment in study area, Colorado River, Grand Canyon National Park, Arizona. *A*, Survey vessel deploying camera system. *B*, Camera system wet end, housed in 46-kilogram split ball (Barnard and others, 2007). *C*, Approximately 1-by-1 centimeter sample image of sand at river mile 30.

Images were taken in a loose grid pattern in areas proximal to the USGS streamgages at RMs 30 and 61. A total of 260 images were collected at 157 unique locations ("stations"). If an unobstructed sand bed was present at a station, five images were collected. No images were collected at stations with rocks, gravel, or other conditions that prevented the viewing window from sitting flush on the bed. Images collected (fig. 4*C*) were about 10 × 7 mm, with a pixel resolution of 0.014 mm. Grain-size

distributions and summary statistics were estimated from each image using the methods and software described by Buscombe (2013). Horizontal station positions were recorded by TS survey by targeting a 360° prism cluster mounted to a 2-m pole affixed to the boom carrying the B-Reel cable. Whereas the survey data have horizontal positional accuracy of 95 percent within 0.031 m, these represent the horizontal position of the prism cluster rather than that of the camera as it contacts the river bed. This "layback" distance and direction from the position of the prism cluster is difficult to measure, especially in areas of fast current. Factors affecting the layback include boat velocity and orientation, along with water depth and velocity. We estimate that layback ranges in magnitude from 0 in calm, shallow locations, to as much as 5 m in deep water with fast current.

Bed-Sediment Classification

Backscatter from the MB survey data were processed using the spectral analysis methods of Buscombe and others (2014a, 2014b) to produce maps of surface sediment type. The backscatter magnitude is computed per beam by balancing the active sonar equation, accounting for losses in acoustic energy due to spherical spreading, attenuation by water and sediment, and physical footprint of the beam. The sediment method classifies heterogeneous riverbed sediments by type (sand, gravel, cobbles/boulders/rock) continuously in space and at 0.25 ×0.25 m grid cell resolution. The process uses backscatter statistics related to georeferenced underwater video observations of the bed. The variance of the power spectrum, and the intercept and slope from a power-law spectral form (termed the spectral strength and exponent, respectively) are used to discriminate between sediment types using a random forest classifier, which is a machine-learning technique that fits decision-tree classifiers on various sub-samples of the data, using averaging to improve the predictive accuracy. Buscombe and others (2014a, 2014b) used these procedures to classify spatially heterogeneous patches of homogeneous sands, gravels (and sand-gravel mixtures), and cobbles/boulders/bedrock with 95-, 88-, and 91-percent accuracy, respectively.

Digital Elevation Models

The TS, MB, and SB data points were combined and used to construct DEMs of the channel bed and banks for the entire study reach in ArcGIS™ version 10.3 (fig. 5; Kaplinski and others, 2014). Where bathymetry data points overlapped, priority was given to the MB data points (fig. 5*A*). This was accomplished by creating a polygon surrounding the MB point data, which was used to clip the SB coverage to erase SB points in areas of overlap. The remaining TS, MB, and SB points were then used to create triangular irregular networks (TINs) from the point data using a Delaunay triangulation (fig. 5*B*; Peuker and others, 1978). Breaklines were incorporated in the TIN models along morphological grade-breaks and other features to accurately represent the topographic surface (see section, "Conventional Total Station Surveys"). The TIN models were edited to ensure that the model best represented the topographic surface and eliminated excessive interpolation. Triangular facets along the outer edge of the TIN model that were greater than about 10 m were eliminated. Contour and shaded relief maps were used to inspect the TIN surface, and any errors detected during data collection (for example, improper rod height coding, crossing breaklines) were edited and additional breaklines were added to ensure proper model formation. The edited TINs for each segment were then used to generate a 1-m resolution raster DEM from the TIN model using linear interpolation (fig 5*C*).

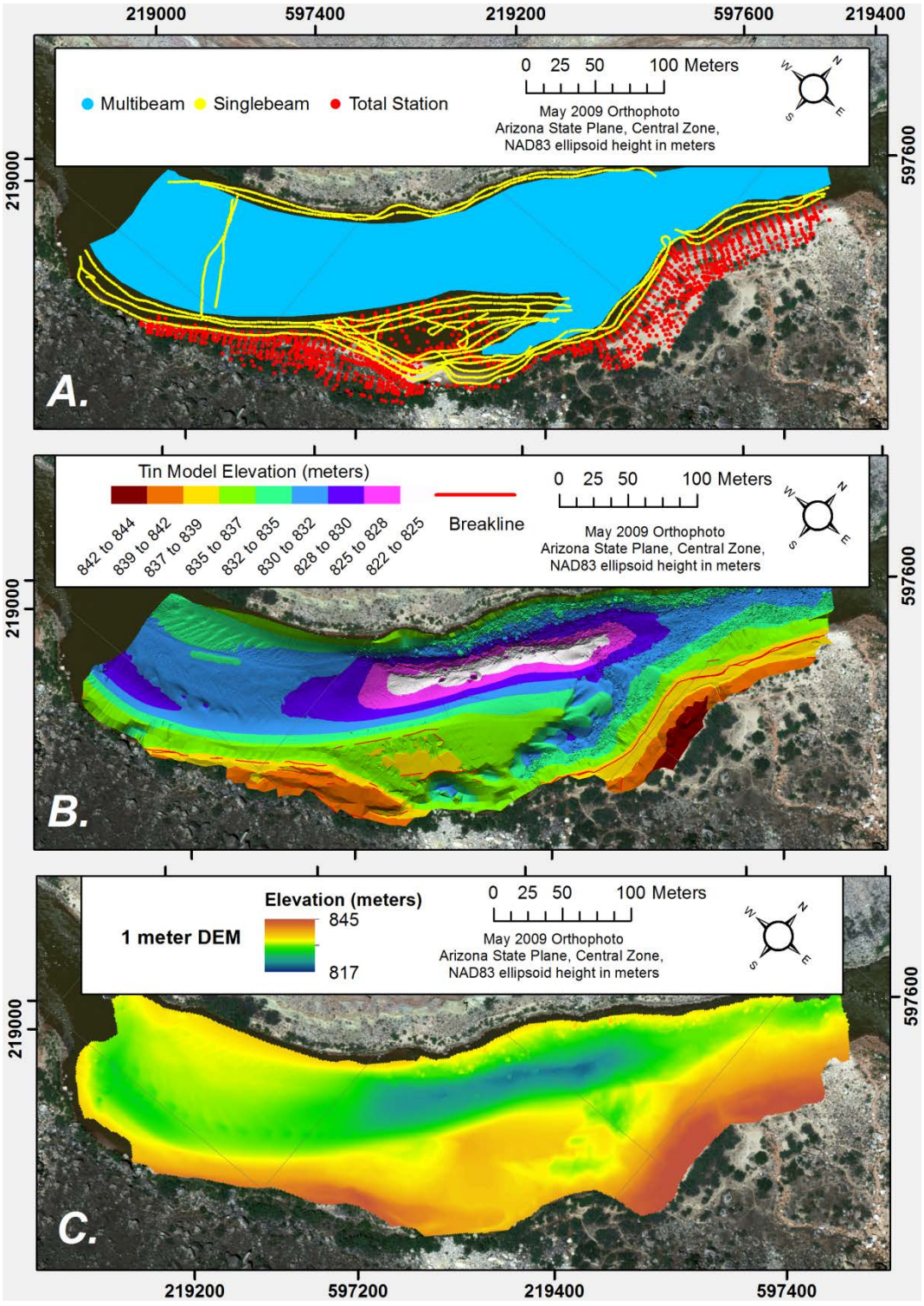

Figure 5. Orthoimages showing steps in digital terrain model construction for study area, Colorado River, Grand Canyon National Park, Arizona. *A,* Survey data points from total station, singlebeam, and multibeam surveys. *B*, Triangular irregular network (TIN) model with breaklines constructed from survey data point files. *C*, 1-meter digital elevation model (DEM) generated from TIN model. Background is 0.2-meter resolution orthophotograph collected in 2009.

Digital Elevation Model Uncertainty

Accounting for elevation uncertainty to reliably differentiate actual geomorphic change from spurious change due to survey and interpolation error is a critical component of monitoring studies that compare sequential DEMs to detect spatial patterns and volumes of morphological change (Brasington and others, 2003; Lane and others, 2003; Wheaton and others, 2010). DEM elevation uncertainty is affected by many factors, including measurement errors associated with the survey methods used, topographic complexity, point density, and interpolation method (Lane, 1998; Heritage and Large, 2009; Wheaton and others, 2010). In this study, we first estimated the measurement uncertainty using quality control checks for each survey method, then used derivative products from the topographic data itself to construct a spatially variable elevation uncertainty model for the DEMs using a fuzzy inference system (FIS).

Measurement Uncertainty

Measurement uncertainty estimates define the minimum level of uncertainty, or the lowest uncertainty attainable using the survey equipment specific to each data-collection type. MB measurement uncertainty was estimated by conducting a performance test at one site located at RM 36.4 (fig. 6). A performance test compares a "check line" dataset with a "reference surface" dataset constructed from narrowly spaced MB data using only beam angles less than 45 degrees (U.S. Army Corps of Engineers, 2013). The reference surface was developed over a relatively flat area with depths of about 6 m. A 0.25 × 0.25 m grid reference surface was constructed by collecting multiple passes over a small patch of the riverbed. Soundings from all passes were filtered to only use soundings with a beam angle of less than 45 degrees, and the median elevation of the soundings in each cell was assigned as the cell elevation. Soundings from a survey line passing through the reference surface were compared to the coincident cell elevation of the reference surface. The results of the performance test show that the MB system has a minimal bias with a mean elevation difference (ME) of -0.005 m, and are highly precise with a mean absolute elevation difference (MAE) of 0.022 m and a 95-percent RMSE of 0.056 m. We use the MAE value as the measurement uncertainty for the MB system (Willmott and Matsuura, 2005).

The measurement uncertainty for SB surveys was estimated by using cross-line checks (U.S. Army Corps of Engineers, 2013). A cross-line check compares the elevation of points that are located within a radius of 0.05 m from separate, intersecting survey lines. We conducted cross-line checks on one SB survey conducted at river mile 42.5 (fig. 7). For each pair of points, the difference in elevation was calculated and the values from all cross-line point pairs were combined to derive an estimate of measurement uncertainty. The results of the cross-line analyses show that the SB system was of good quality with a ME of -0.003 m (indicating minimal bias), a MAE of 0.021 m, and 95-percent RMSE of 0.061 m, which meet both U.S. Corps of Engineers and International Hydrographic Office standards for "special order" and surveys (U.S. Army Corps of Engineers, 2013).

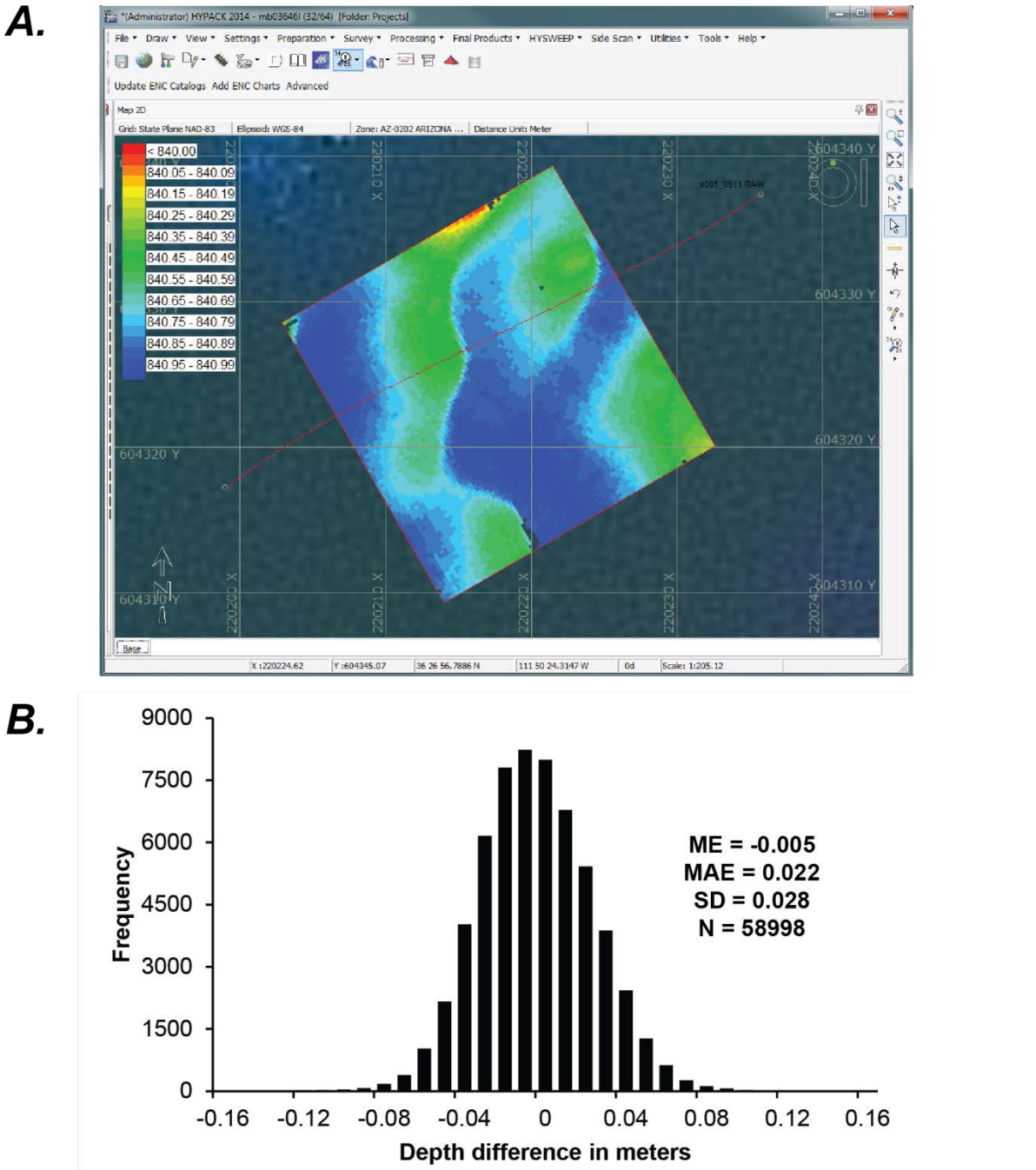

Figure 6. Results of multibeam survey performance test comparing the vertical difference between a check line with a reference surface at river mile 36.4, Colorado River, Grand Canyon National Park, Arizona. *A*, Image showing reference surface and location of check line. *B*, Histogram showing vertical difference between reference surface and check line. Reference surface is created by surveying a small patch of relatively flat area with multiple, overlapping survey lines using only beam angles less than 45 degrees.

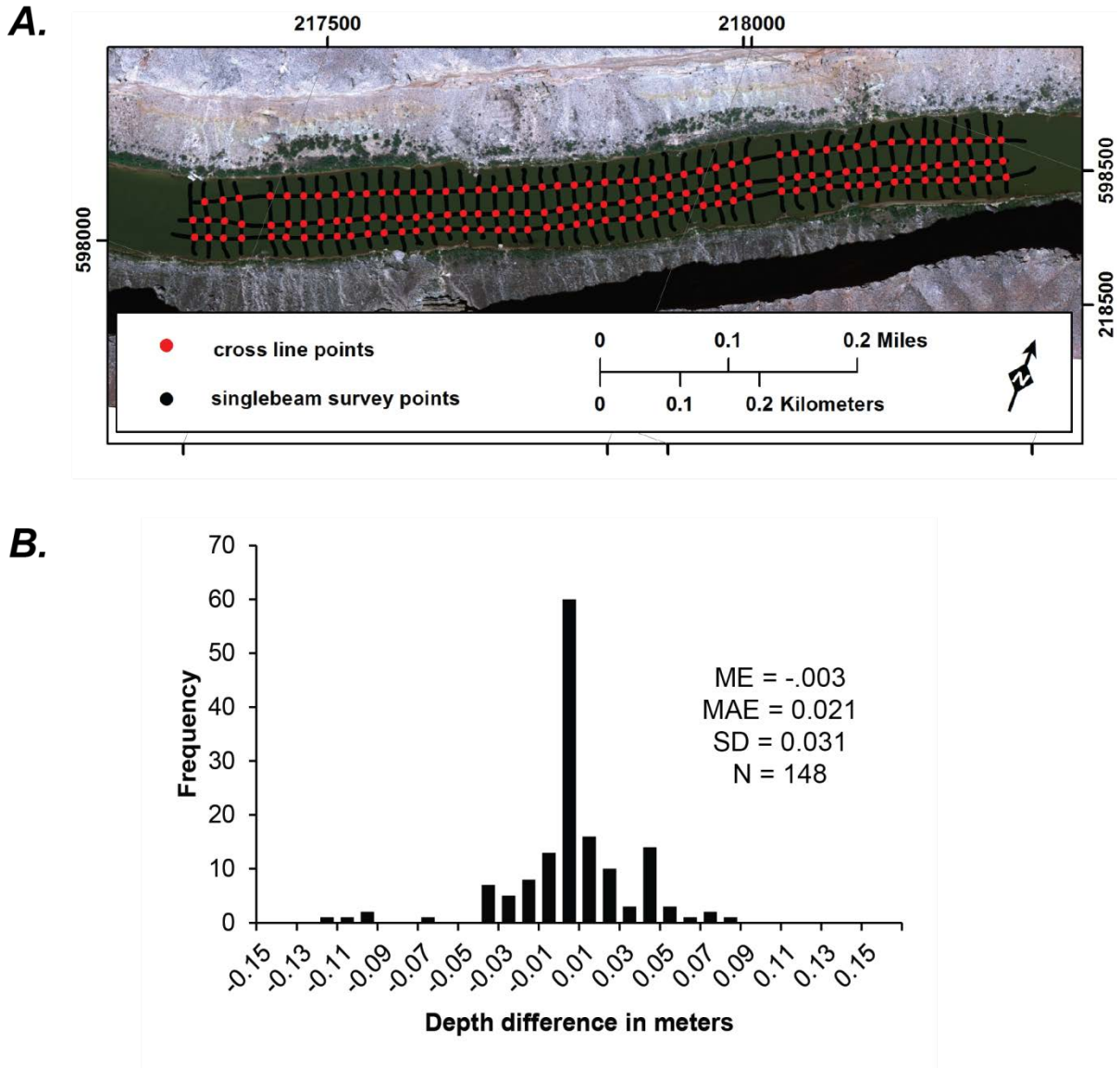

Figure 7. Singlebeam survey cross-line checks at river mile 42.5, Colorado River, Grand Canyon National Park, Arizona. *A*, Image showing location of cross-line points. *B,* Histogram showing difference between cross-line check points. Cross-line analysis compares the elevation (depth) of points at intersecting survey lines. Points within a radius of 0.05 meter from separate survey lines were used.

The measurement uncertainty associated with the TS surveys was estimated by using the results from an empirical study. In this study, an extendable survey rod was targeted by a TS at each extension whilst plumbed over a control point, and the difference in elevation between the TS observation and control point elevation was used to estimate the measurement uncertainty. A total of 193 observations were collected at 40 different sites and show that the stations had the lowest measurement uncertainty of the data-collection types used in this study, with a ME of 0.004 m, a MAE of 0.008 m, and a 95 percent RMSE of 0.021 m. We used the MAE, rounded to the nearest centimeter, or 0.01 m, as the measurement uncertainty associated with the TS surveys.

Fuzzy Inference System Elevation Uncertainty Model

A FIS uses combinations of known parameters, or inputs, that affect survey or interpolation accuracy, to generate a single elevation uncertainty estimate on a pixel-by-pixel basis using empirically derived values and knowledge-based relationships between inputs and uncertainty. We used the Geomorphic Change Detection (http://gcd.joewheaton.org/) software plugin to ArcGIS™ version 10.3 and followed the procedures outlined by Wheaton and others (2010) and Bangen and others (2016) to develop and apply the FIS error models. Input and output variable ranges are binned into membership functions (MFs) that are subdivided into classes (in this study, up to four classes were used—"low", "medium", "high", and "extreme") based on the statistical distribution of the input variable observed across the study site. For any combination of input variables, applicable MFs are selected and combined using a rule table to yield a fuzzy estimate of elevation uncertainty (for example , 'low', 'medium', 'high', 'extreme'). The rule table codifies all combinations of input MF relationships and determines the location on the output elevation uncertainty MF. For example, if a survey area has a relatively low slope, high point density, and low interpolation uncertainty, it should have a relatively low elevation uncertainty. In contrast, areas with higher slopes, lower point densities, and higher interpolation uncertainty should have a relatively higher elevation uncertainty. This fuzzy elevation uncertainty is then translated into a crisp (for example, numeric) uncertainty estimate by computing the centroid of the applicable elevation uncertainty MF(s).The elevation uncertainty output is calculated for each grid cell and tabulated in a raster surface, concurrent with the DEM. A detailed discussion of FIS error modeling is available in Wheaton and others (2010), Jang and Gully (2014), Bangen and others (2016), and the Geomorphic Change Detection Web site (http://gcd.joewheaton.org/).

The process of constructing a FIS involves (1) defining input variables and MFs, (2) defining output categories and calibrating the MFs to independent estimates of error, and (3) defining the rules that relate the various combination of MF inputs to the output estimate of elevation uncertainty. The data-collection areas were defined by generating a polygon surrounding each set of input data points and merging the polygons to outline the entire study reach. Three FIS models were developed, one for each area of data collection (MB, SB, TS). The FIS model for MB sonar survey areas used four input MFs, (namely, slope, interpolation error, point density, and roughness, [fig. 8]), whereas the FIS models for SB and TS survey areas used three input MFs (slope, interpolation error, and point density [figs. 9, 10]). All the FISs developed in this study use a Mamdani FIS type, minimum rule implication method, maximum aggregation method, centroid defuzzification method, and trapezoidal MF shape (Jang and Gully, 2014).

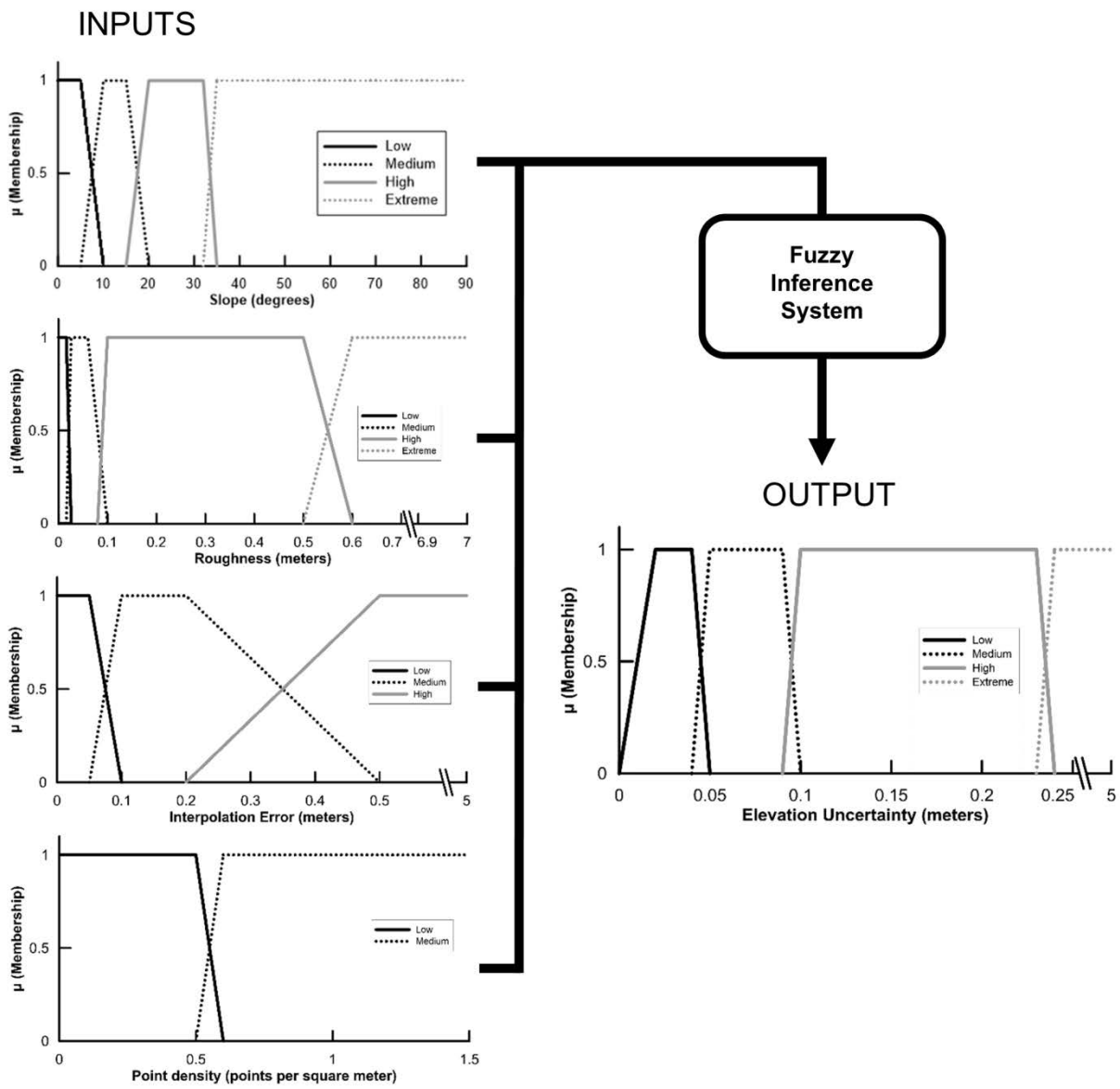

Figure 8. Diagram of fuzzy inference system model for multibeam sonar survey areas showing input and output membership functions. Inputs are slope, interpolation error, point density, and roughness. Output is elevation uncertainty. Note the variable x-axis breaks in both input and output functions.

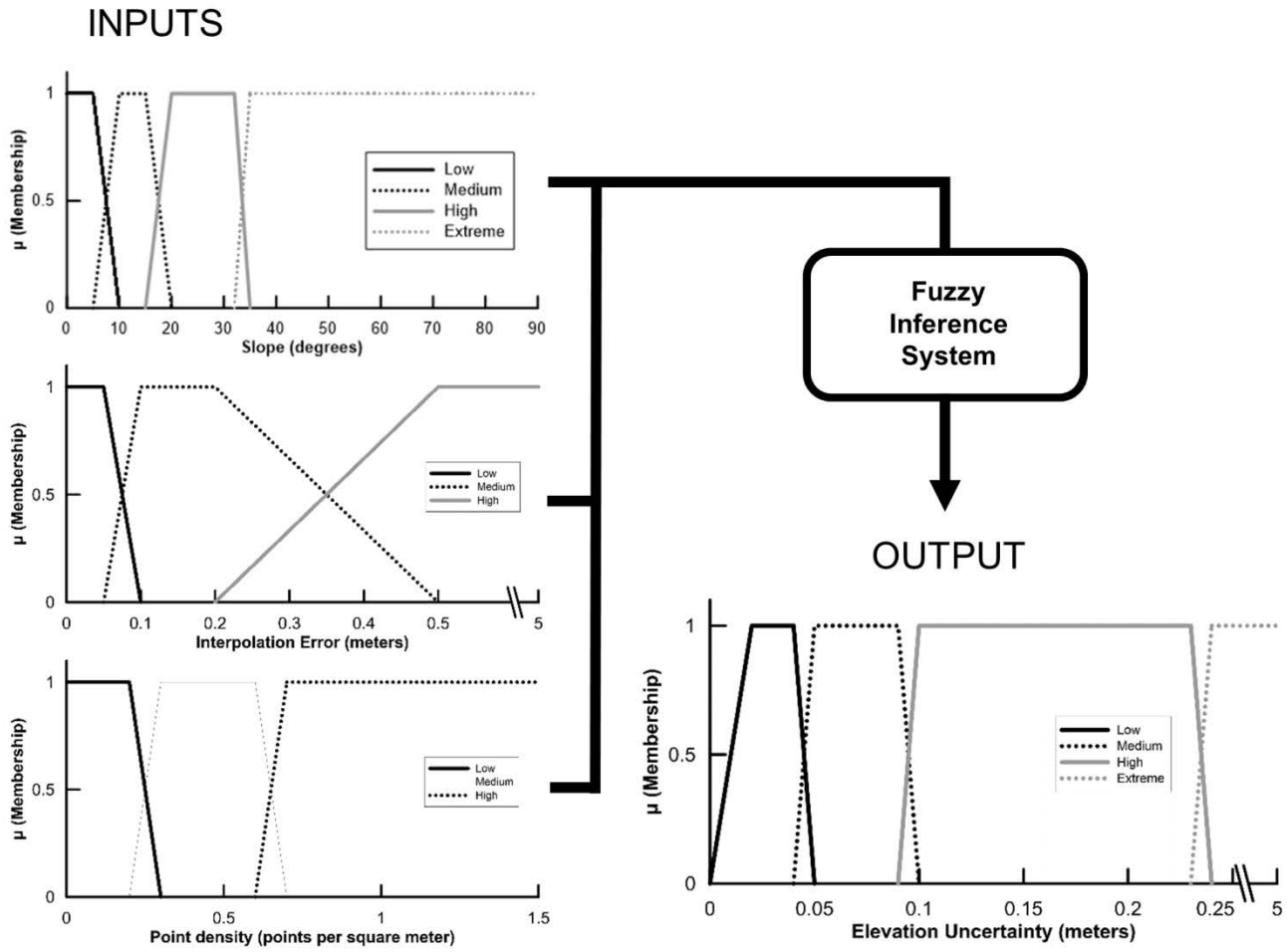

Figure 9. Diagram of fuzzy inference system model for singlebeam sonar survey areas showing input and output membership functions. Inputs are slope, interpolation error, and point density. Output is elevation uncertainty. Note the variable x-axis breaks in both input and output functions.

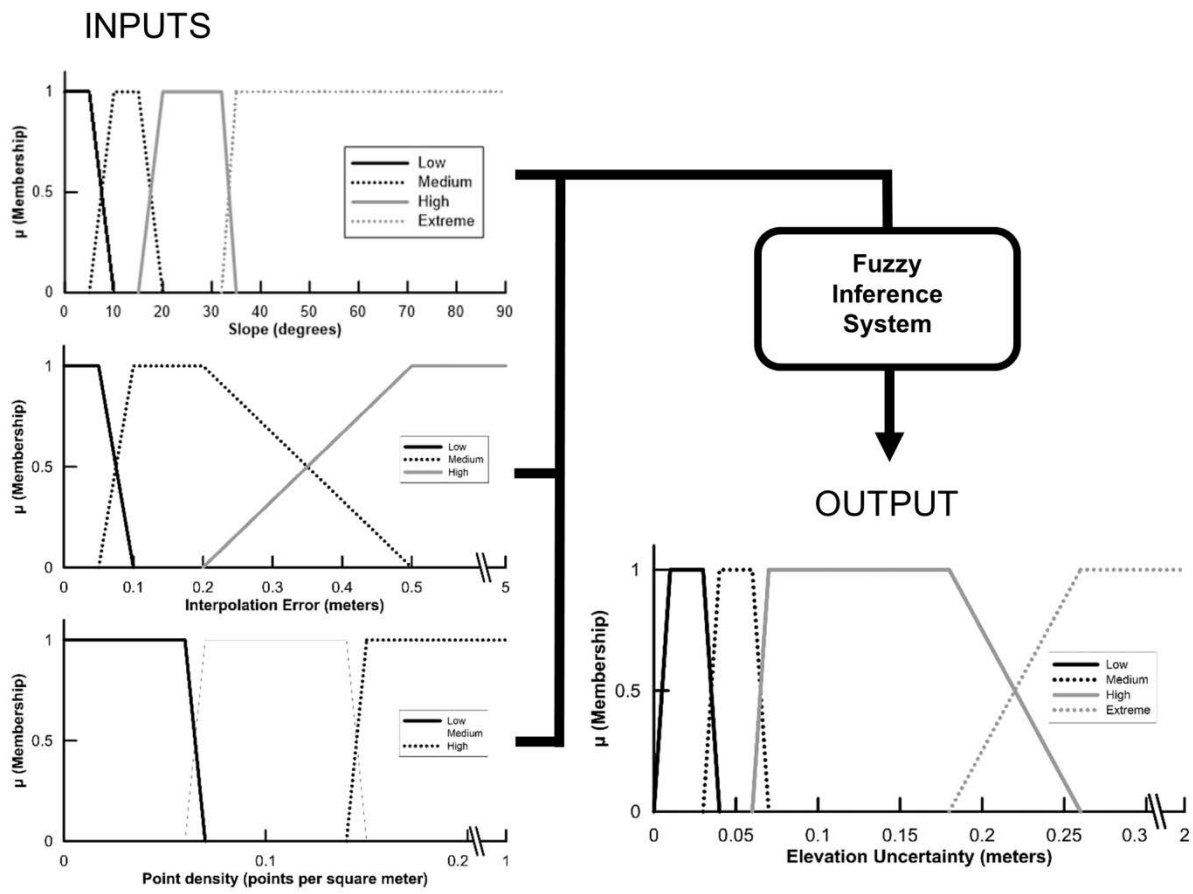

Figure 10. Diagram of fuzzy inference system for total station survey areas showing input and output membership functions. Inputs are slope, interpolation error, and point density. Output is elevation uncertainty. Note the variable x-axis breaks in both input and output functions.

Fuzzy Inference System Input

Input MFs were derived by using raster surfaces of slope, point density, interpolation error, and roughness generated from the survey point data and resultant DEM (fig. 11). Input MFs for each survey method were calibrated to the range of input in each of the survey areas and divided into two to four categories, depending on the input variable. In FIS models, MF category boundaries intentionally overlap and are designed to encompass a range of values; thus, they are particularly useful when we think that the boundaries between membership classes are not strictly defined (for example , "low" compared to "medium" slope). When the input value of a particular cell lies in the overlap region between two different categories, the FIS model uses the centroid defuzzification method to transfer a certain percentage of value from each category within which that the value lies. For example, if an input cell value lies exactly in the center of the overlap region between a low and medium category, then the FIS will transfer 50 percent of a low category and 50 percent of the medium category to the output MF.

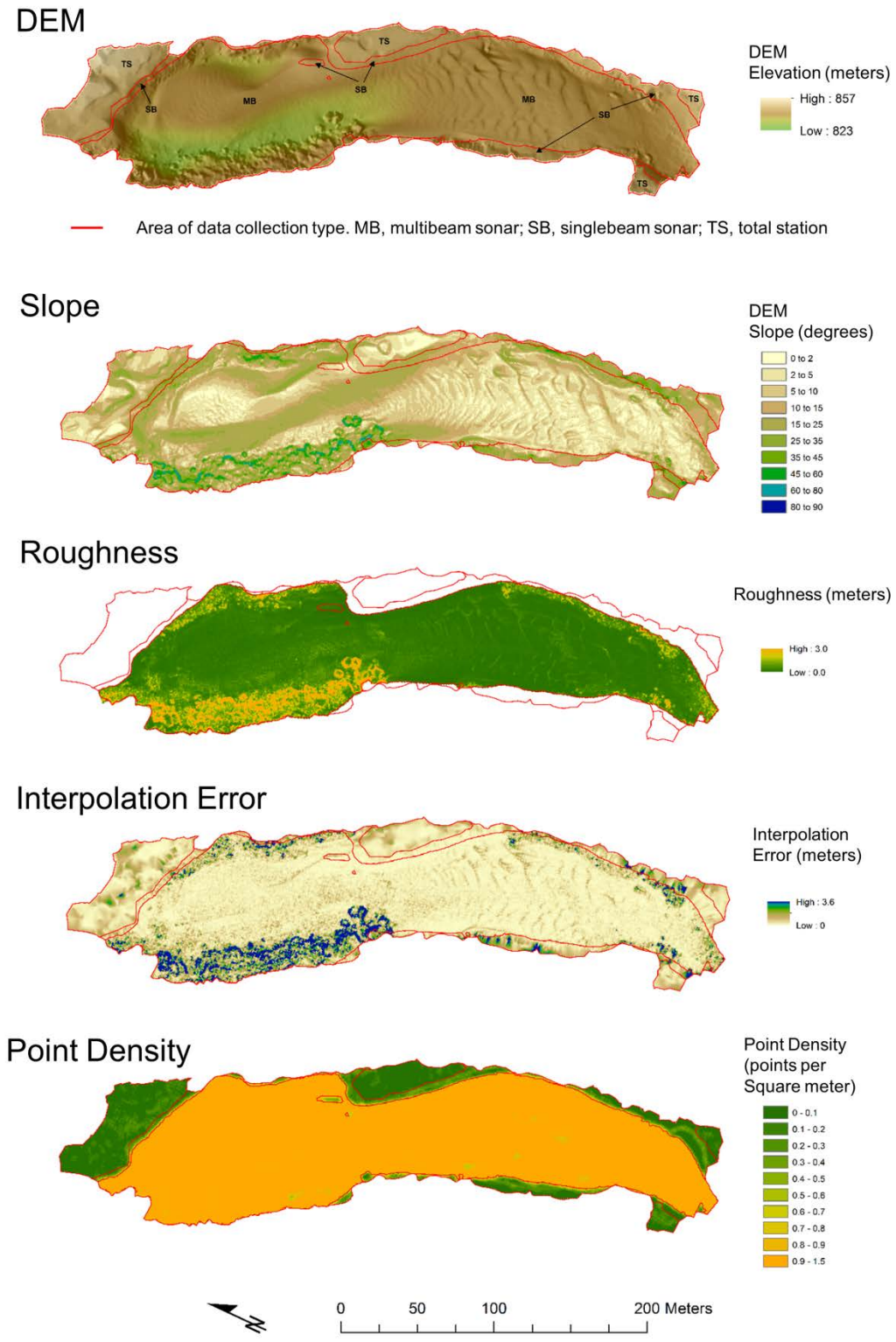

Figure 11. Images showing digital elevation model (DEM), slope, point density, interpolation error, and roughness raster surfaces used to derive the fuzzy inference system input membership functions, for an approximately 0.5-kilometer section of study reach located at river mile 34.9, Colorado River, Grand Canyon National Park, Arizona.

Slope

The contribution of topographic complexity to elevation uncertainty was modeled by using the surface slope for all three survey methods. Elevation uncertainty generally increases with slope because in steep areas, small horizontal position errors can lead to large differences in point elevation. DEM surface slope in degrees was derived for each 1-m grid cell by calculating the maximum rate of elevation change within a 3 × 3 cell neighborhood (fig. 12; Wheaton and others, 2010).

The study reach has a wide range of slopes, ranging from 0 to 82 degrees (slopes exceeding angle of repose are rock surfaces), and all three areas of data collection have similar population distributions. Therefore, we used the same input MF for all three data-collection areas. The slope input MFs used four categories (low, medium, high, and extreme; fig.12), and the boundary between each category was defined by using statistical parameters from the slope population distribution. For the boundary between the low and medium categories, we used the average median value (7.9 degrees) of the three slope populations (MB, SB, and TS). The boundary between the medium and high categories was centered on the third quartile of the populations (17 degrees), and the boundary between the high and extreme categories was defined using the 95-percent percentile of the population (33 degrees). The extreme category encompasses slope values from 33 to 90 degrees.

Roughness

Surface roughness also was used as a representation of surface complexity, but only for the MB survey part of the FIS. Point densities are too low within the SB and TS parts of the DEMs to generate a usable surface roughness parameter for these survey methods. We used the locally detrended standard deviation as a proxy for surface roughness and calculated surface roughness using the Topographic Point Cloud Analysis Toolkit (ToPCAT; Brasington and others, 2012; Rychkov and others, 2012) embedded in the GCD ArcGIS™ plugin. The locally detrended standard deviation was calculated for each 1-m grid cell using the 0.25-m grid of MB elevations (fig. 13).

The distribution of roughness values shows that the channel bed primarily is comprised of a relatively smooth surface, with smaller areas of extremely complex topography (fig. 13). Roughness values ranged from 0 to 6.771 m, with a median value of 0.026 m. We used a four-category input MF (low, medium, high, and extreme; fig. 13) to capture the range of complexity within the channel. The boundary between the low and medium categories was defined by the median value of the population (0.026 m), the third quartile (0.06 m) was used for the boundary between the medium and high categories, and the 99th percentile was used to define the boundary between the high and extreme categories.

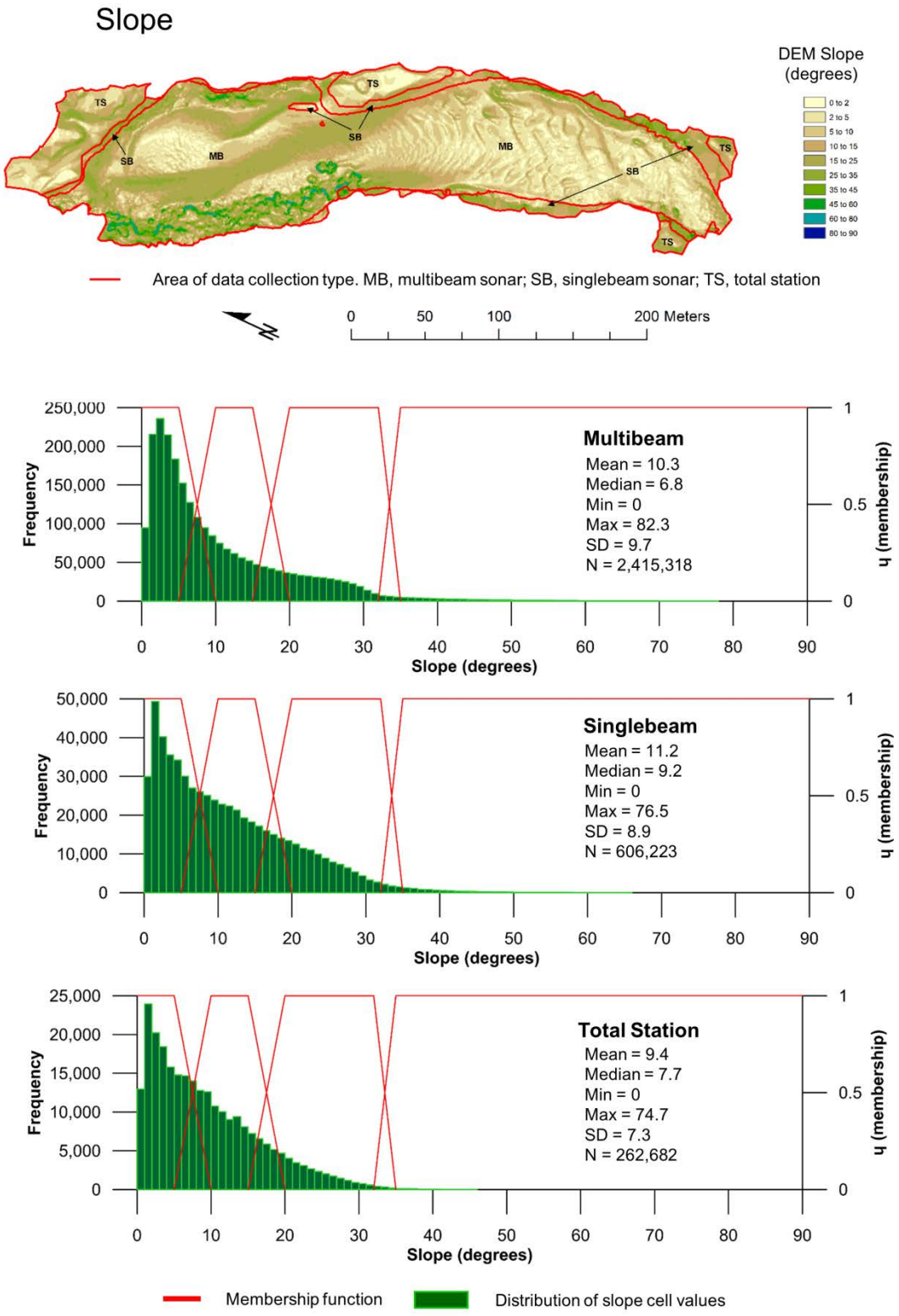

Figure 12. Image showing 1-meter slope raster for an approximately 0.5-kilometer section of study reach and plots for each data-collection area with histograms of distribution of cell values and the input membership function used in the fuzzy inference system model, on the Colorado River, Grand Canyon National Park, Arizona.

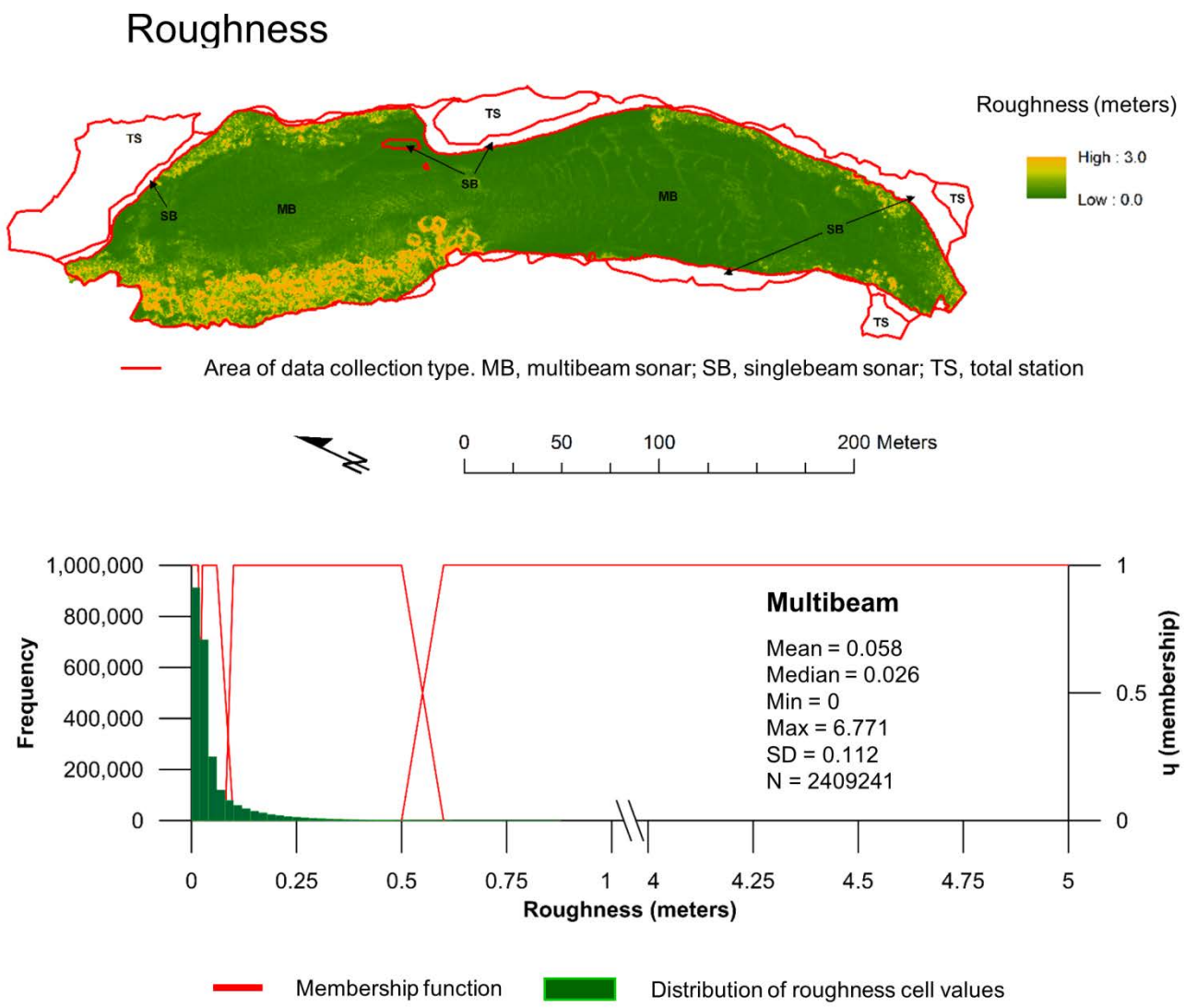

Figure 13. Image showing 1-meter roughness raster for an approximately 0.5-kilometer section of the study reach and plots for each data-collection area with histogram of distribution of cell values and the input membership function used in fuzzy inference system model, on the Colorado River, Grand Canyon National Park, Arizona.

Interpolation Uncertainty

Interpolation uncertainty represents the error introduced during interpolation of the irregularly spaced points that are explicitly represented in the TIN model to produce a regularly spaced grid of elevations (for example, a raster DEM). Interpolation uncertainty was derived by calculating the elevation difference between the final DEM and input point data (fig. 14).

Interpolation uncertainty values were relatively low for most of the DEM, with isolated areas of relatively high values. Interpolation uncertainty distributions were similar for all data-collection areas and the same input MF was used for all three areas. Interpolation uncertainty values ranged from 0 to 5.796 m, with median values ranging from 0.016 to 0.032 m (fig. 14). Schwendel and others (2012) reported that errors associated with converting from TIN to raster generally are low, and our findings concur with their conclusions. The wide range of interpolation uncertainty values was modeled with a three-category MF (low, medium, and extreme; fig.14).

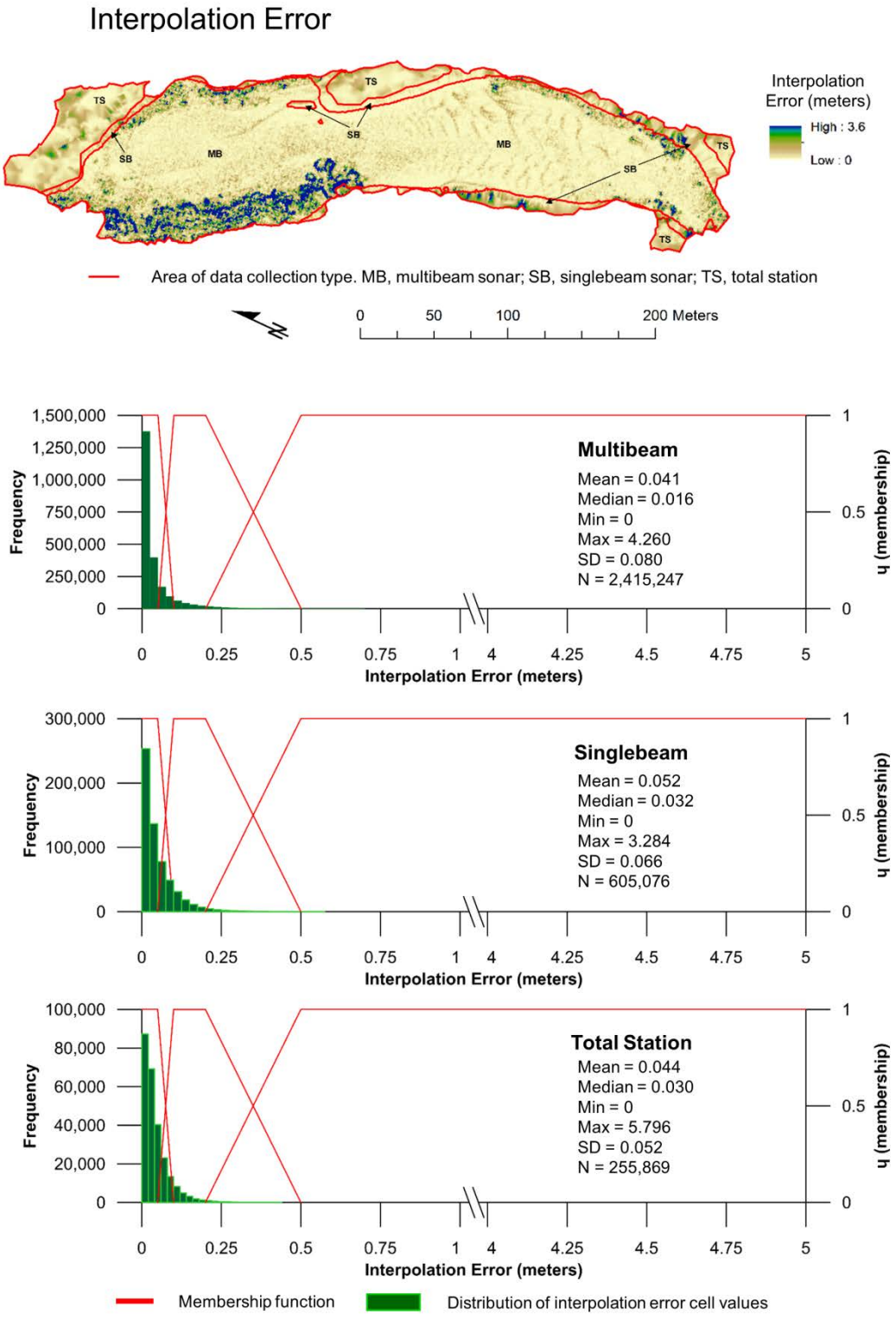

Figure 14. Image showing 1-meter interpolation uncertainty raster for an approximately 0.5-kilometer section of study reach and plots for each data-collection area with histograms of distribution of cell values and the input membership function used in fuzzy inference system model, on the Colorado River, Grand Canyon National Park, Arizona.

Point Density

Differences in point density arise as a result of the different sampling strategies of each data-collection method. Point density was calculated from the survey point cloud using a 5-m radius circular neighborhood (fig. 15). The three data-collection methods have unique distributions, and separate input MFs were developed for each data-collection area.

MB soundings for each individual survey were decimated to a 1-m point grid and used in DEM construction. The distribution of point density in the MB survey area reflects this scheme and has a narrow distribution, with a median value of 1 point per square meter (pts/m^2). Areas with higher point densities are from locations where MB surveys overlapped, and areas with lower point densities are from gaps in the MB coverage. Low point density areas typically occur in shallow sand or gravel bars with relatively low slope and roughness where the MB footprint is narrow. In these areas, surveyors chose to forgo full coverage for survey efficiency and equipment safety. A two-category MF (low, high; fig. 15) was used to transfer areas of low point density (that is, gaps in coverage) to higher elevation uncertainties.

SB points typically occur as a line of points along the survey vessel track line. As a result, SB data-collection areas have a wide range of point density values (0–1.2 pts/m^2), with a median value of 0.16 pts/m^2. A three-category MF (low, medium, high; fig. 15) was created to capture the range of SB point densities. The boundary between the low and medium category was defined by the median value of the population, and the boundary between medium and high categories were defined by the mean plus 2 standard deviations.

TS data-collection areas have the lowest point densities, with a median value of 0.04 pts/m^2. A three-category MF (low, medium, high; fig. 15) was used to capture the range of TS point density values. The boundary between the low and medium categories was defined by the mean point density value (0.06 pts/m^2), and the mean plus two standard deviations was used to define the boundary between the medium and high categories.

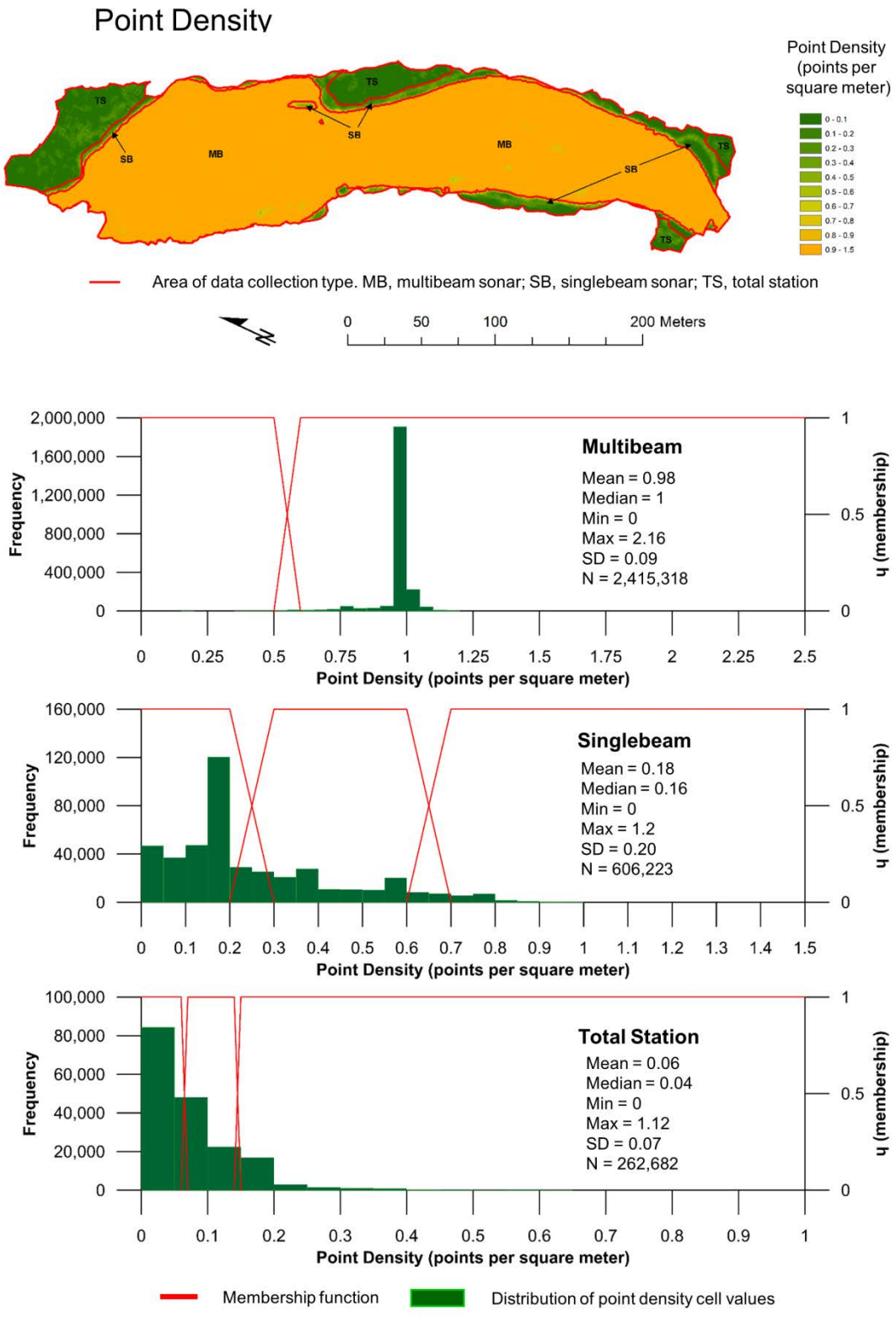

Figure 15. Image showing 1-meter point density raster for an approximately 0.5-kilometer section of study reach and plots for each data-collection area with histograms of distribution of cell values and the input membership function used in the fuzzy inference system model, on the Colorado River, Grand Canyon National Park, Arizona.

Fuzzy Inference System Output

The FIS output elevation uncertainty MFs are used in combination with the rules table to generate a single elevation uncertainty estimate for each cell. Defining the output elevation uncertainty categories is an iterative process that incorporates expert knowledge of the survey methods and the terrain surveyed, and that is calibrated to an independent estimate of elevation uncertainty. The minimum, or lower end of the output categories, was defined by estimating the measurement uncertainty for each data-collection type. The maximum elevation uncertainty was set to the maximum local relief observed in the study reach for each data-collection type. Other category boundaries ("low", "medium", "high", and "extreme") were defined by empirical relationships pertinent to each data-collection type.

Once the minimum (individual measurement uncertainty) and maximum (bank height) levels were established, the output MFs for each data-collection type were calibrated to an independent source of uncertainty. For MB and SB sonar, we used a derivative of the raw sounding point cloud to calibrate the output MFs. Before the MB sonar data was incorporated in the DEMs, the raw sounding point cloud was decimated to a 1-m grid by assigning the median value of the sounding elevations to each cell center. Summary statistics for each cell also were calculated, and we used the standard deviation of the sounding elevations for each 1-m grid cell as a proxy for elevation uncertainty (fig. 16). Output MFs were defined by the distribution of the standard deviation dataset from an MB survey located at river mile 34.9 and applied to the entire study reach. This site contains a wide variety of channel bed features and complexity that are characteristic of the entire study reach. The "low" category begins at the measurement uncertainty estimation (0.02 m) and the boundary between the low and medium categories was defined as the median value of the standard deviation population (0.040 m). The boundary between the medium and high categories was defined by the third quartile (0.09 m) of the population, whereas the boundary between the high and extreme categories is defined by the 95th-percentile value of the population. The use of quartiles and percentiles offers an objective means to assign boundaries for any similar dataset. The "extreme" MF begins at the 95th percentile to the maximum value of 5 m based on maximum local relief. Because SB survey areas do not have an independent source of uncertainty, we used the MB output MFs for SB survey areas. TS data were calibrated using the values derived by Wheaton and others (2010). Rule tables were developed for each FIS (tables 1–3) and used in combination with the FIS input and output MFs to generate a spatially distributed elevation uncertainty surface of the entire study reach (fig. 17).

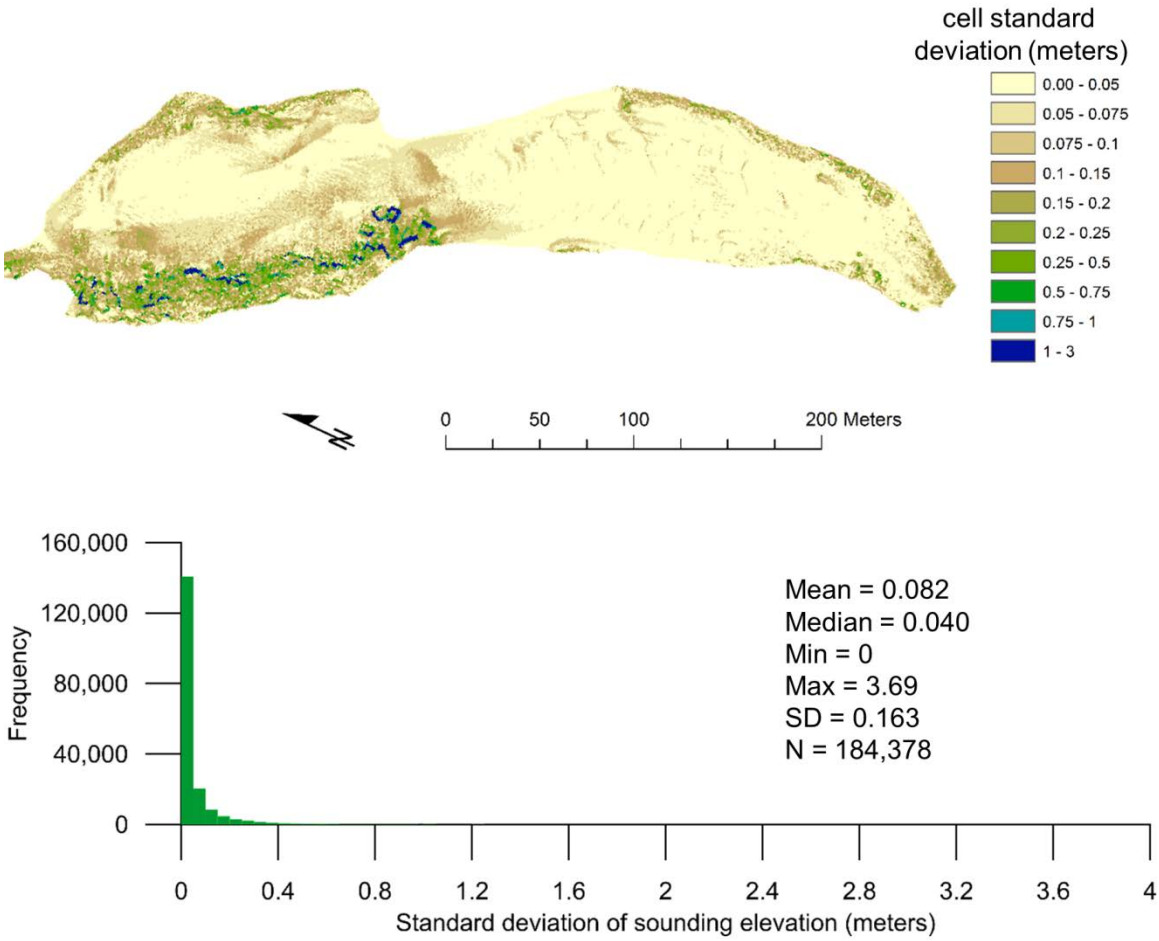

Figure 16. Image showing standard deviation of soundings within each 1-meter cell and graph showing distribution, and summary statistics of dataset from multibeam survey collected at river mile 34.9, Colorado River, Grand Canyon National Park, Arizona.

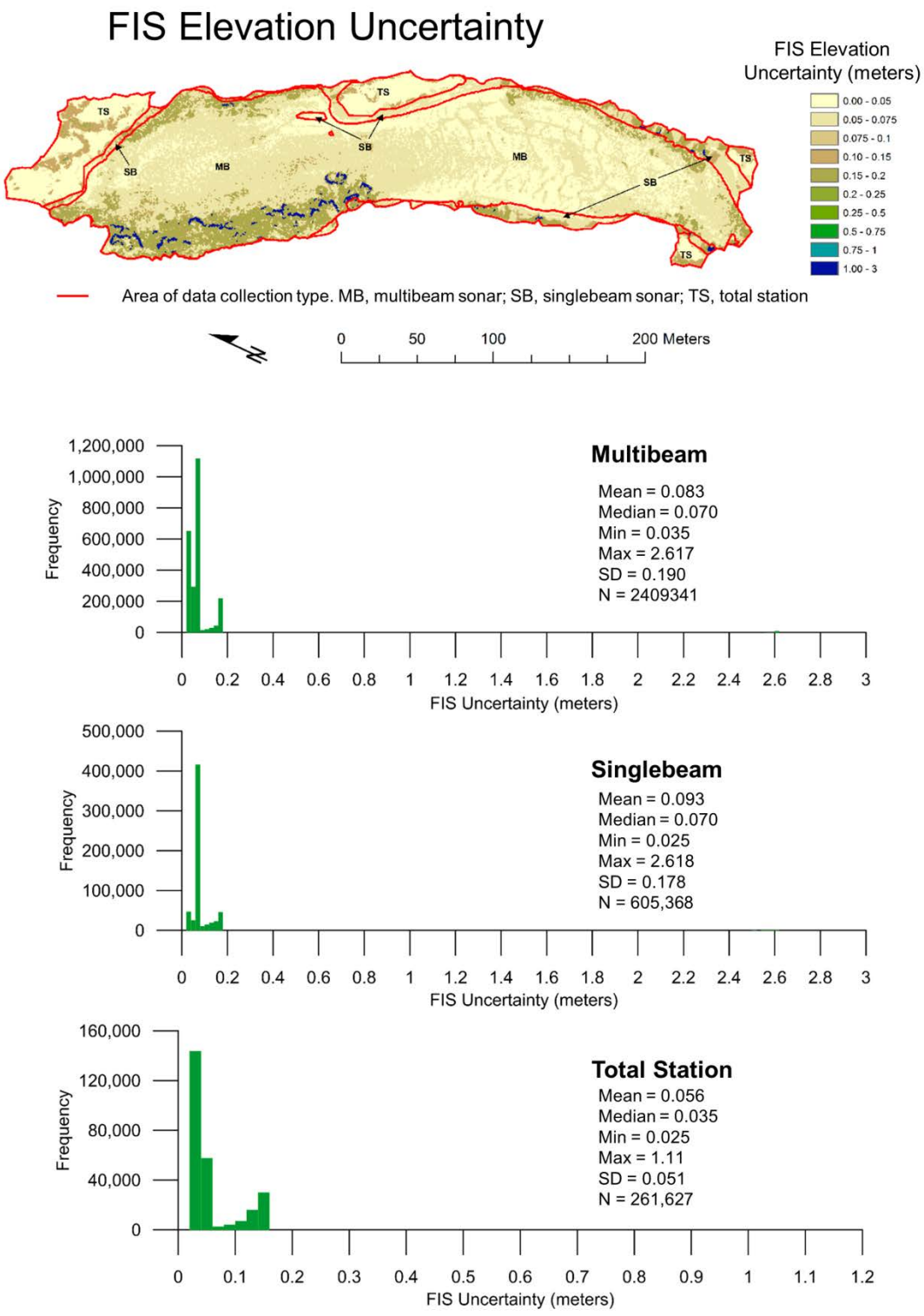

Figure 17. Image of fuzzy inference system (FIS) elevation uncertainty output, and graphs showing distributions and summary statistics of dataset segregated by survey type, for the study reach on the Colorado River, Grand Canyon National Park, Arizona.

Table 1. Three-input fuzzy inference system ruleset for total station surveys.

Rule	Inputs			Output (meters)
	Slope (degrees)	Interpolation (meters)	Point density (points per square meter)	
1	Low	Low	Low	Low
2	Low	Medium	Low	Medium
3	Low	High	Low	High
4	Low	Low	Medium	Low
5	Low	Medium	Medium	Medium
6	Low	High	Medium	Medium
7	Low	Low	High	Low
8	Low	Medium	High	Medium
9	Low	High	High	Medium
10	Medium	Low	Low	Medium
11	Medium	Medium	Low	High
12	Medium	High	Low	High
13	Medium	Low	Medium	Low
14	Medium	Medium	Medium	Medium
15	Medium	High	Medium	High
16	Medium	Low	High	Low
17	Medium	Medium	High	Medium
18	Medium	High	High	High
19	High	Low	Low	High
20	High	Medium	Low	High
21	High	High	Low	High
22	High	Low	Medium	Medium
23	High	Medium	Medium	High
24	High	High	Medium	High
25	High	Low	High	Medium
26	High	Medium	High	High
27	High	High	High	High
28	Extreme	Low	Low	High
29	Extreme	Medium	Low	High
30	Extreme	High	Low	Extreme
31	Extreme	Low	Medium	High
32	Extreme	Medium	Medium	High
33	Extreme	High	Medium	Extreme
34	Extreme	Low	High	Medium
35	Extreme	Medium	High	High
36	Extreme	High	High	Extreme

Table 2. Three-input fuzzy inference system ruleset for singlebeam sonar surveys.

Rule	Inputs			Output (meters)
	Slope (degrees)	Interpolation (meters)	Point Density (points per square meter)	
1	Low	Low	Low	Medium
2	Low	Medium	Low	Medium
3	Low	High	Low	High
4	Low	Low	Medium	Low
5	Low	Medium	Medium	Medium
6	Low	High	Medium	Medium
7	Low	Low	High	Low
8	Low	Medium	High	Medium
9	Low	High	High	Medium
10	Medium	Low	Low	Medium
11	Medium	Medium	Low	Medium
12	Medium	High	Low	High
13	Medium	Low	Medium	Low
14	Medium	Medium	Medium	Medium
15	Medium	High	Medium	High
16	Medium	Low	High	Low
17	Medium	Medium	High	Medium
18	Medium	High	High	High
19	High	Low	Low	Medium
20	High	Medium	Low	High
21	High	High	Low	High
22	High	Low	Medium	Medium
23	High	Medium	Medium	High
24	High	High	Medium	High
25	High	Low	High	Medium
26	High	Medium	High	High
27	High	High	High	High
28	Extreme	Low	Low	High
29	Extreme	Medium	Low	High
30	Extreme	High	Low	Extreme
31	Extreme	Low	Medium	Medium
32	Extreme	Medium	Medium	High
33	Extreme	High	Medium	Extreme
34	Extreme	Low	High	Medium
35	Extreme	Medium	High	High
36	Extreme	High	High	Extreme

Table 3. Four-input fuzzy inference system ruleset for multibeam sonar surveys.

Rule	Inputs				Output (meters)
	Slope (degrees)	Roughness (meters)	Interpolation (meters)	Point density (points per square meter)	
1	Low	Low	Low	Low	Medium
2	Low	Low	Low	High	Low
3	Low	Medium	Low	Low	Medium
4	Low	Medium	Low	High	Medium
5	Low	High	Low	Low	High
6	Low	High	Low	High	Medium
7	Low	Extreme	Low	Low	High
8	Low	Extreme	Low	High	High
9	Low	Low	Medium	Low	Medium
10	Low	Low	Medium	High	Low
11	Low	Medium	Medium	Low	Medium
12	Low	Medium	Medium	High	Medium
13	Low	High	Medium	Low	High
14	Low	High	Medium	High	High
15	Low	Extreme	Medium	Low	High
16	Low	Extreme	Medium	High	High
17	Low	Low	High	Low	Medium
18	Low	Low	High	High	Medium
19	Low	Medium	High	Low	Medium
20	Low	Medium	High	High	Medium
21	Low	High	High	Low	High
22	Low	High	High	High	High
23	Low	Extreme	High	Low	High
24	Low	Extreme	High	High	High
25	Medium	Low	Low	Low	Medium
26	Medium	Low	Low	High	Low
27	Medium	Medium	Low	Low	Medium
28	Medium	Medium	Low	High	Medium
29	Medium	High	Low	Low	Medium
30	Medium	High	Low	High	Medium
31	Medium	Extreme	Low	Low	High
32	Medium	Extreme	Low	High	High
33	Medium	Low	Medium	Low	Medium
34	Medium	Low	Medium	High	Medium
35	Medium	Medium	Medium	Low	Medium
36	Medium	Medium	Medium	High	Medium
37	Medium	High	Medium	Low	High
38	Medium	High	Medium	High	High
39	Medium	Extreme	Medium	Low	High
40	Medium	Extreme	Medium	High	High
41	Medium	Low	High	Low	High
42	Medium	Low	High	High	High
43	Medium	Medium	High	Low	High
44	Medium	Medium	High	High	High
45	Medium	High	High	Low	High
46	Medium	High	High	High	High
47	Medium	Extreme	High	Low	High
48	Medium	Extreme	High	High	High
49	High	Low	Low	Low	Medium
50	High	Low	Low	High	Low

Rule	Inputs				Output (meters)
	Slope (degrees)	Roughness (meters)	Interpolation (meters)	Point density (points per square meter)	
51	High	Medium	Low	Low	Medium
52	High	Medium	Low	High	Medium
53	High	High	Low	Low	High
54	High	High	Low	High	High
55	High	Extreme	Low	Low	High
56	High	Extreme	Low	High	High
57	High	Low	Medium	Low	Medium
58	High	Low	Medium	High	Medium
59	High	Medium	Medium	Low	Medium
60	High	Medium	Medium	High	Medium
61	High	High	Medium	Low	High
62	High	High	Medium	High	High
63	High	Extreme	Medium	Low	High
64	High	Extreme	Medium	High	High
65	High	Low	High	Low	High
66	High	Low	High	High	High
67	High	Medium	High	Low	High
68	High	Medium	High	High	High
69	High	High	High	Low	High
70	High	High	High	High	High
71	High	Extreme	High	Low	High
72	High	Extreme	High	High	High
73	Extreme	Low	Low	Low	Medium
74	Extreme	Low	Low	High	Low
75	Extreme	Medium	Low	Low	Medium
76	Extreme	Medium	Low	High	Medium
77	Extreme	High	Low	Low	High
78	Extreme	High	Low	High	High
79	Extreme	Extreme	Low	Low	Extreme
80	Extreme	Extreme	Low	High	Extreme
81	Extreme	Low	Medium	Low	Medium
82	Extreme	Low	Medium	High	Medium
83	Extreme	Medium	Medium	Low	Medium
84	Extreme	Medium	Medium	High	Medium
85	Extreme	High	Medium	Low	High
86	Extreme	High	Medium	High	High
87	Extreme	Extreme	Medium	Low	Extreme
88	Extreme	Extreme	Medium	High	Extreme
89	Extreme	Low	High	Low	High
90	Extreme	Low	High	High	High
91	Extreme	Medium	High	Low	High
92	Extreme	Medium	High	High	High
93	Extreme	High	High	Low	High
94	Extreme	High	High	High	High
95	Extreme	Extreme	High	Low	Extreme
96	Extreme	Extreme	High	High	Extreme

Results

The first goal of this study was to collect the data necessary to produce a high-resolution DEM of the study area. This goal was achieved on an 18-day, self-supported research river trip that consisted of 5 motor-powered rafts and 23 personnel. A total of 51 MB surveys, 54 SB surveys, 90 TS surveys, and 260 bed-sediment grain-size measurements were collected. In addition to topographic data, the TS surveys placed temporary benchmarks, completed a line-of-sight traverse of the entire study area between geodetic control network benchmarks, and constrained locations of the underwater grain-size measurements.

A 1-m resolution DEM of a 33-mi (53-km) reach of the Colorado River between RMs 29 and 62 within GRCA was created from MB and SB sonar, and TS surveys. The DEM covers an area of 3.28 km^2 and about 85 percent of the channel, by area within the study reach. Surveys were not conducted in rapids, riffles, and some selected shallow gravel bar areas. MB surveys covered 74 percent of the DEM area, and SB and TS surveys covered 18 percent and 8 percent, respectively. The DEMs are available in digital format (Kaplinski and others, 2017).

A 1-m resolution grid of spatially distributed uncertainty also was created to accompany the DEM by using FIS modeling. For the MB survey area, the four-input parameter FIS model produced per-cell elevation uncertainties that ranged from 0.035 to 2.617 m, with a mean of 0.083 m. The SB survey areas show the highest average uncertainties, with a mean of 0.093 m. Uncertainties within the TS area show a mean of 0.056 m. The FIS uncertainty estimates also are presented in digital format (Kaplinski and others, 2017).

Bed-sediment classification maps were produced that discriminate between three sediment types—sands, gravels, and cobbles/boulders/bedrock—using the methods of Buscombe and others (2014a, 2014b). Processed grain-size data from the underwater camera system and the bed sediment-classifications are presented in digital format (Kaplinski and others, 2017).

Summary

One-meter digital elevation models (DEMs) were constructed for a 30-mile (48-kilometer) study reach along the Colorado River in Grand Canyon National Park, Arizona. The DEMs combine elevations determined from ground-based total station (TS) surveys, and boat-based bathymetric sonar surveys collected on a research river trip during May 6–19, 2009. TS surveys were used to measure the riverbank topography, position temporary benchmarks, and collect supplemental observations on geodetic control network points. Most of the study area was mapped using the multibeam (MB) sonar system. Gaps in MB coverage, particularly near the shoreline areas, were surveyed with the singlebeam (SB) sonar system. TS surveys of topography focused on describing the topography of active sandbars, water-surface elevations, and shallow offshore locations to tie in with the bathymetric survey data.

The general approach to DEM construction was to create a triangular irregular network (TIN) model from the input datasets, and then generate a 1-meter raster DEM from the TIN model. The DEM and associated surfaces (slope, roughness, points density, interpolation uncertainty) used in the uncertainty analysis were co-registered at exact northing and easting coordinates, which ensured that the cells from each surface would overlap exactly with cells from another surface (that is, concurrency).

Estimates of elevation uncertainty were derived using a fuzzy inference system (FIS). FISs were developed for each type of data collection (MB sonar, SB sonar, and TS surveys) and were used to generate a spatially variable elevation uncertainty surface.

Bed-sediment maps were constructed for the entire area surveyed by MB sonar at a 0.25-meter resolution that classify sediments into three categories corresponding to the Wentworth classes of sand, gravel, and undifferentiated cobble/boulder/bedrock.

The results from this study will inform ongoing efforts to assess the effects of Glen Canyon Dam operations on the status and trends of sediment resources in the Colorado River ecosystem. The DEMs and bed-sediment classifications will be used by researchers to map the spatial characteristics of geomorphic change within the study reaches and to estimate sediment budgets for different time periods by calculating volumetric differences between surveys. Additionally, the data will provide valuable information to hydraulic and morphodynamic models, as well assist in the delineation of the spatial distribution of benthic habitat for food-base and fisheries investigations.

Acknowledgments

This study was made possible by the hard work of the numerous members of the field survey team. In particular, we thank Rod Parnell, Nathan Schott, Pete Jensen, Hoda Sondossi, Laura Kennedy, Karen Koestner, and Meagan Polino for their great attitude and expert survey work. We thank the boatmen of Humphrey Summit Support—Brian Dierker, Pete Weiss, Stuart Reeder, Tim Cooper, and Lynn Roeder—for their expertise in the field. Tom Gushue offered extensive database and GIS services and Geoff Chain contributed many hours of processing in the laboratory.

References Cited

Bangen, S., Hensleigh, J., McHugh, P., and Wheaton, J., 2016, Error modeling of DEMs from topographic surveys of rivers using fuzzy inference systems: Water Resources Research, v. 52, no. 2, p. 1,176–1,193, doi:10.1002/2015WR018299.

Barnard, P.L., Rubin, D.M., Harney, J., and Mustain, N., 2007, Field test comparison of an autocorrelation technique for determining grain size using a digital ‘beachball’ camera versus traditional methods: Sedimentary Geology, v. 201, p. 180–195, doi:10.1016/j.sedgeo.2007.05.016.

Brasington, J., Vericat, D., and Rychkov, I., 2012, Modeling river bed morphology, roughness, and surface sedimentology using high resolution terrestrial laser scanning: Water Resources Research, v. 48, no. 11, doi:10.1029/2012wr012223.

Brasington J, Langham, J., and Rumsby, B., 2003, Methodological sensitivity of morphometric estimates of coarse fluvial sediment transport: Geomorphology, v. 53, p. 299–316.

Buscombe, D., 2013, Transferable wavelet method for grain-size distribution from images of sediment surfaces and thin sections, and other natural granular patterns: Sedimentology, v. 60, no. 7, p. 1,709–1,732, doi:10.1111/sed.12049.

Buscombe, D., Grams, P.E., and Kaplinski, M.A., 2014a, Characterizing riverbed sediment using high-frequency acoustics 1—Spectral properties of scattering: Journal of Geophysical Research—Earth Surface, v. 119, no. 12, p. 2,674–2,691, doi:10.1002/2014JF003189.

Buscombe, D., Grams, P.E., and Kaplinski, M.A., 2014b, Characterizing riverbed sediment using high-frequency acoustics 2—Scattering signatures of Colorado River bed sediment in Marble and Grand Canyons: Journal of Geophysical Research—Earth Surface, v. 119, no. 12, p. 2,692–2,710, doi:10.1002/2014JF003191.

Chezar, H., and Rubin, D., 2004, Underwater microscope system: U.S. Patent and Trademark Office, patent number 6,680,795, January 20, 2004, 9 p.

Doyle, D.R., 1994, Development of the National Spatial Reference System: Silver Spring, Maryland, National Geodetic Survey, http://www.ngs.noaa.gov/PUBS_LIB/develop_NSRS.html.

Grams, P.E., Schmidt, J.C., Wright, S.A., Topping, D.J., Melis, T.S., and Rubin, D.M., 2015, Building sandbars in the Grand Canyon: EOS, v. 96, no. 11, p. 12–16, https://eos.org/features/building-sandbars-in-the-grand-canyon.

Grams, P.E., Topping, D.J., Schmidt, J.C., Hazel, J.E., Jr., and Kaplinski, M.A., 2013, Linking morphodynamic response with sediment mass balance on the Colorado River in Marble Canyon—Issues of scale, geomorphic setting, and sampling design: Journal of Geophysical Research—Earth Surface, v. 118, no. 2, p. 361–381, http://dx.doi.org/10.1002/jgrf.20050.

Hazel, J.E., Jr., Kaplinski, M., Parnell, R.A., Kohl, K., and Schmidt, J.C., 2008, Monitoring fine-grained sediment in the Colorado River ecosystem, Arizona—Control network and conventional survey techniques: U.S. Geological Survey Open-File Report 2008-1276, 15 p.

Heritage, G., and Large, A.R.G., eds., 2009, Laser scanning for the environmental sciences: Chichester, United Kingdom, Wiley.

Jang, J., and Gulley, N., 2014, Fuzzy logic toolbox—User guide: Natick, Massachusetts, Mathworks, 328 p.

Kaplinski, M., Hazel, J.E., Jr., Grams, P.E., and Davis, P., 2014, Monitoring fine-sediment volume in the Colorado River ecosystem, Arizona—Construction and analysis of digital elevation models: U.S. Geological Survey Open-File Report 2009-1207, 29 p.

Kaplinski, M., Hazel, J.E. Jr., Grams, P.E., Kohl, Keith, Buscombe, D.D., and Tusso, R.B., 2017, Channel mapping of the Colorado River in Grand Canyon National Park, Arizona, May 2009, river miles 29 to 62—Data: U.S. Geological Survey data release, https://dx.doi.org/10.5066/F7930RCG.

Kaplinski, M., Hazel, J.E., Jr., Parnell, R., Breedlove, M., Kohl, K., and Gonzales, M., 2009, Monitoring fine-sediment volume in the Colorado River ecosystem, Arizona—Bathymetric survey techniques: U.S. Geological Survey Open-File Report 2014-1052, 41 p.

Lane, S.N., 1998, The use of digital terrain modelling in the understanding of dynamic river channel systems, *in* Lane, S.N., Richards, K., and Chandler, J., eds., Landform monitoring, modelling, and analysis: Chichester, United Kingdom, Wiley, p. 311–342.

Lane, S.N., Westaway, R.M., and Hicks, D.M., 2003, Estimation of erosion and deposition volumes in a large, gravel-bed, braided river using synoptic remote sensing: Earth Surface Processes and Landforms, v. 28, p. 249–271.

Mueller, E.R., Grams, P.E., Schmidt, J.C., Hazel, J.E., Jr., Alexander, J.S., and Kaplinski, M., 2014, The influence of controlled floods on fine sediment storage in debris fan-affected canyons of the Colorado River Basin: Geomorphology, v. 226, p. 65–75, http://dx.doi.org/10.1016/j.geomorph.2014.07.029.

Peuker, T.K., Fowler, R.J., Little, J.J., and Mark, D.M., 1978, The triangulated irregular network, Proceedings of the Digital Terrain Models (DTM) Symposium, St. Louis: American Society of Photogrammetry, p. 516–540.

Rubin, D.M., Chezar, H., Harney, J.N., Topping, D.J., Melis, T.S., and Sherwood, C.R., 2007, Underwater microscope for measuring spatial and temporal changes in bed-sediment grain size: Sedimentary Geology, v. 202, p. 402–408.

Rubin, D.M., Topping, D.J., Schmidt, J.C., Hazel, J., Kaplinski, K., and Melis, T.S., 2002, Recent sediment studies refute Glen Canyon Dam hypothesis: EOS, Transactions, American Geophysical Union, v. 83, no. 25, p. 273 and 277–278.

Rychkov, I., Brasington, J., and Vericat, D., 2012, Computational and methodological aspects of terrestrial surface analysis based on point clouds: Computers and Geosciences, v. 42, p. 64–70, doi:10.1016/j.cageo.2012.02.011.

Saleh, R.A., Chayes, D.N., Dasler, J.L., Doyle, D.R., Sanchez, R., Renslow, M.S., and Rose, J.J., 2003, Survey protocol evaluation program—Final report submitted to the Grand Canyon Monitoring and Research Program, accessed August 17, 2008, at http://www.gcmrc.gov/library/reports/GIS/Saleh2003.pdf.

Schmidt, J. C., and Graf, J.B., 1990, Aggradation and degradation of alluvial sand deposits, 1965 to 1986, Colorado River, Grand Canyon National Park, Arizona: U.S. Geological Survey Professional Paper 1493, 74 p.

Schmidt, J.C., Topping, D.J., Grams, P.E., and Hazel, J.E., 2004, System-wide changes in the distribution of fine sediment in the Colorado River corridor between Glen Canyon Dam and Bright Angel Creek, Arizona—Final report: Logan, Utah State University, submitted to U.S. Geological Survey, Grand Canyon Monitoring and Research Center, Cooperative Agreement No. 1425-98-FC-22640, 107 p., http://www.gcmrc.gov/library/reports/Physical/Fine_Sed/Schmidt2004.pdf.

Schwendel, A.C., Fuller, I.C., and Death, R.G., 2012, Assessing DEM interpolation methods for effective representation of upland stream morphology for rapid appraisal of bed stability: River Research and Applications, v. 28, no. 5, p. 567–584.

Stem, J. E., 1989, State Plane Coordinate System of 1983, National Oceanic and Atmospheric Administration Manual NOS NGS 5, v.5, 119 p., https://www.ngs.noaa.gov/PUBS_LIB/ManualNOSNGS5.pdf.

Topping, D.J., Rubin, D.M., Nelson, J.M., Kinzel, P.J., III, and Corson, I.C., 2000, Colorado River sediment transport—Part 1—Natural sediment supply limitation and the influence of Glen Canyon Dam: Water Resources Research, v. 36, p. 515–542.

Topping, D.J., Schmidt, J.C., and Vierra, L.E., Jr., 2003, Computation and analysis of the instantaneous-discharge record for the Colorado River at Lees Ferry, Arizona—May 8, 1921, through September 30, 2000: U.S. Geological Survey Professional Paper 1677, 118 p.

U.S. Army Corps of Engineers, 2013, Hydrographic surveying, engineer manual EM 1110-2-1003: U.S Army Corps of Engineers, 506 p., accessed May 21, 2015, at http://www.publications.usace.army.mil/Portals/76/Publications/EngineerManuals/EM_1110-2-1003.pdf.

U.S. Geological Survey, 2006, Colorado mileage system—Spatial database GIS.BASE_GCMRC_TenthMile (1st revised ed.): U.S. Geological Survey Grand Canyon Monitoring and Research Center, accessed June 16, 2006, at http://www.gcmrc.gov/products/ims.

Wheaton, J.M., Brasington, J., Darby, S.E., and Sear, D.A., 2010, Accounting for uncertainty in DEMs from repeat topographic surveys—Improved sediment budgets: Earth Surface Processes and Landforms, v. 35, p. 136–156, doi: 10.1002/esp.1886.

Willmott, C. J., and Matsuura, K., 2005, Advantages of the mean absolute eror (MAE) over the root mean square error (RMSE) in assessing average model performance: Climate Research, v. 30, p. 79–82.

Wright, S.A., and Kaplinski, M., 2011, Flow structures and sandbar dynamics in a canyon river during a controlled flood, Colorado River, Arizona: Journal of Geophysical Research, v. 116, no. F01019, 15 p., http://www.agu.org/pubs/crossref/2011/2009JF001442.shtml.

Wright, S.A., Melis, T.S., Topping, D.J., and Rubin, D.M., 2005, Influence of Glen Canyon Dam operations on downstream sand resources of the Colorado River in Grand Canyon, *in* Gloss, S.P., Lovich, J.E., and Melis, T.S., eds., The state of the Colorado River ecosystem in Grand Canyon: U.S. Geological Survey Circular 1282, p. 17–31.

Wright, S.A., Schmidt, L.C., Melis, T.S., Topping, D.J., and Rubin, D.M., 2008, Is there enough sand?—Evaluating the fate of Grand Canyon sandbars: GSA Today, v. 18, no. 8.

Zilkoski, D.B., D'Onofrio, J.D., and Frakes, S.J., 1997, Guidelines for establishing GPS-derived ellipsoid heights (Standards—2 cm and 5 cm), version 4.3: Silver Spring, Maryland, National Oceanic and Atmospheric Administration Technical Memorandum NOS NGS-58, National Geodetic Survey, 22 p.

Publishing support provided by the U.S. Geological Survey
Science Publishing Network, Menlo Park and Tacoma Publishing Service Centers

For more information concerning the research in this report, contact the
GCMRC Staff, Southwest Biological Science Center
U.S. Geological Survey Grand Canyon Monitoring and Research Center
2255 N. Gemini Drive
Flagstaff, Arizona 86001
https://www.gcmrc.gov/

ISSN 2331-1258 (online)
https://doi.org/10.3133/ofr20171030